reactions

MDPI

Article

Diels–Alder Cycloaddition of *N*-Azobenzene Maleimides with Furan and Electrochemical Study of Redox Reactions

David Fernando Venegas-Villalvazo [1], David Abraham Figueroa-Hernández [1], Armando Pineda-Contreras [1,*], José Manuel Flores-Alvarez [1], Héctor García-Ortega [2] and Juan Saulo González-González [3]

[1] Facultad de Ciencias Químicas, Universidad de Colima, Carretera Colima-Coquimatlán s/n, Coquimatlán 28400, Colima, Mexico; dvenegas@ucol.mx (D.F.V.-V.); davidabraham_figueroa@ucol.mx (D.A.F.-H.); josemanuel@ucol.mx (J.M.F.-A.)
[2] Facultad de Química, Universidad Nacional Autónoma de México, Mexico City 04510, Mexico; hector.garcia@unam.mx
[3] Instituto de Farmacobiología, Universidad de la Cañada, Carretera Teotitlán-San Antonio Nanahuatipán, km 1.7 s/n, Teotitlán de Flores Magón 68540, Oaxaca, Mexico; juan_saulo@unca.edu.mx
* Correspondence: armandop@ucol.mx

Abstract: This work reports the synthesis of aminoazobenzene compounds derived from 3,5-dimethylaniline (**1a**–**1f**) via a diazo-coupling reaction with aromatic amines. These aminoazobenzenes were acylated with maleic anhydride to obtain the corresponding maleimides (**2a**–**2f**). The maleimides were then used as dienophiles in a Dies–Alder cycloaddition reaction with furan as the diene, yielding the adducts (**3a**–**3f**). All synthesized compounds were characterized using FTIR, ^{1}H, and ^{13}C NMR spectroscopy. Additionally, electrochemical studies using cyclic voltammetry were conducted to determine the oxidation–reduction reactions present in the compounds.

Keywords: Diels–Alder reactions; azocompounds; electrochemical studies; maleimides

Citation: Venegas-Villalvazo, D.F.; Figueroa-Hernández, D.A.; Pineda-Contreras, A.; Flores-Alvarez, J.M.; García-Ortega, H.; González-González, J.S. Diels–Alder Cycloaddition of *N*-Azobenzene Maleimides with Furan and Electrochemical Study of Redox Reactions. *Reactions* **2024**, *5*, 928–946. https://doi.org/10.3390/reactions5040049

Academic Editors: Donatella Giomi, Alberto Brandi and Fabrizio Machetti

Received: 13 September 2024
Revised: 11 November 2024
Accepted: 13 November 2024
Published: 15 November 2024

1. Introduction

The classical Dies–Alder [1] reaction is one of the best-known and most established reactions in organic chemistry, consisting of a highly selective [4+2] cycloaddition between a conjugated diene and an alkene (dienophile) to yield six-membered ring derivatives with up to four stereogenic centers [2–4]. The Dies–Alder reaction employs maleimide systems as dienophiles to yield dicarboximide derivatives [3–5]. Some dicarboximides are used as agricultural fungicides, including vinclozolin, iprodione, and procymidone [6–8]. Dicarboximides are believed to inhibit triglyceride biosynthesis in sclerotia-forming fungi, such as *Botrytis cinerea* [9,10], and succinate dehydrogenase [11]. *N*-octyl bicycloheptene dicarboximide is an active ingredient in insect repellents [12–14] and certain common pesticides [15–17]. While it has no intrinsic pesticidal activity, it acts as a synergist, enhancing the potency of pyrethroid ingredients. It is used in various household and veterinary products [4,10,15,17].

Other dicarboximide arylene derivatives, due to their high photochemical stability, ease of synthetic modification, and desirable optical/redox characteristics, have applications in field-effect transistors [18–21], molecular electronics [22–24], light-harvesting arrays [25–28], solar cells [28–31], light-emitting diodes [32–34], and fluorescent labeling [35–37]. Azo-organic materials, on the other hand, are well known for their responsiveness to environmental changes. Azo chromophores are characterized by the presence of an azo group (-N=N-) in their molecular structure. Given their applications across various fields, along with their utility as dyes, the synthesis of azo-organic materials is generating considerable interest. Researchers have shown interest in the potential applications of these compounds in optics and optoelectronics, including information storage [38–42], nonlinear optics [43–47], and photorefractive polymers [48,49], among others. Dicarboximides functionalized with azocompounds have been investigated for their ability to

enhance optical properties and thermal stability in certain polymer matrices [50]. Such compounds are also used as photo-switches for the glutamate receptor [51,52], modulating DNA–protein interactions [53].

Cyclic voltammetry and other electrochemical techniques are now indispensable for studying organic compounds. These techniques provide precise detection [54–57] and insights into reactivity [58], mechanisms [59–61], and redox properties [62–64] across a diverse range of chemical species, including pharmaceuticals, inorganics, and polymers. In this context, the present study aims to report the synthesis of new maleimidoazobenzene derivatives and their Dies–Alder reaction with furan, alongside a cyclic voltammetry study of the resulting adducts.

2. Materials and Methods

2.1. General Synthesis of Azocompounds

The synthesis of azocompounds **1a**–**1f** was carried out by the diazotization of the corresponding aromatic amines. In all cases, 8.26 mmol of amines was dissolved in a water–hydrochloric acid mixture (10 mL H_2O:1.5 mL HCl). The mixture was cooled to 0 °C and kept under constant stirring. To this cold reaction mixture, 8.26 mmol of solid sodium nitrite was added slowly with stirring and allowed to react for 15 min. After the diazotation reaction, the nitrosonium ion was neutralized by adding urea using the potassium iodide starch test. Then, 8.26 mmol of 3,5-dimethylaniline hydrochloride dissolved in 10 mL of water was added slowly while controlling the temperature (0–5 °C). Afterward, solid sodium acetate was added to the mixture until it reached an alkaline pH (7–8). The resulting solid was filtered, dried, and recrystallized from ethanol.

2.1.1. (E)-1-(4-((4-Amino-2,6-dimethylphenyl)diazenyl)phenyl)ethan-1-one (**1a**)

The title compound was obtained as thin reddish crystals, with 81% yield and a melting point of 100–102 °C. ^{1}H NMR (400 MHz, DMSO-d6): δ 8.07 (d, *J* = 8.6 Hz, 2H, CH=C-COCH$_3$), 7.77 (d, *J* = 8.6 Hz, 2H, CH=C-N=N), 6.37 (s, 2H, CH=C-NH$_2$), 6.14 (s, 2H, NH$_2$), 2.62 (s, 3H, COCH$_3$), 2.48 (s, 6H, CH$_3$). ^{13}C NMR (101 MHz, DMSO-d6): δ 197.67 (C=O), 156.64, 152.52, 140.04, 138.07, 136.64, 129.92, 121.80, 114.59 (Ar), 27.26 (COCH$_3$), 21.87 (CH$_3$). FTIR (cm^{-1}): 3357 (ν_{as}, N-H), 3209 (ν_{si} N-H), 3016 (ν =C-H), 2954, 2914 (ν C-H), 1668 (ν C=O), 1596, 1469 (ν C=C), 1487 (ν N=N), 1369 (ν C-H), 1355 (ν C-N), 1024 (ν_{Inp} =C-H), 802 (ν_{op}, =C-H). Anal. Calcd. for $C_{16}H_{17}N_3O$ (267.33): C, 71.89%; H, 6.41%; and N, 15.72%. Found: C, 71.80%; H, 6.30%; and N, 15.61 %.

2.1.2. (E)-1-(3-((4-Amino-2,6-dimethylphenyl)diazenyl)phenyl)ethan-1-one (**1b**)

The title compound was obtained as thin orange crystals, with 78% yield and a melting point of 98–100 °C. ^{1}H NMR (400 MHz, $CDCl_3$): δ 8.39 (t, *J* = 1.8 Hz, 1H, CH=C-N=N), 8.02 (d, *J* = 1.9 Hz, 1H, CH=C-COCH$_3$), 8.00 (d, *J* = 1.9 Hz, 1H, CH-C-N=N), 7.59 (t, *J* = 7.8 Hz, 1H, CH-CH), 6.46 (m, 2H, CH=C-NH$_2$), 3.95 (s, 2H, NH$_2$), 2.71 (s, 3H, COCH$_3$), 2.55 (t, *J* = 0.6 Hz, 6H, CH$_3$). ^{13}C NMR (101 MHz, $CDCl_3$): δ 197.85 (C=O), 153.78, 148.06, 142.28, 138.08, 136.66, 129.18, 128.74, 125.68, 122.70, 115.31 (Ar), 26.74 (COCH$_3$), 20.84 (CH$_3$). FTIR (cm^{-1}): 3444 (ν_{as} N-H), 3348 (ν_{si} N-H), 3215 (ν =C-H), 2964, 2914 (ν C-H), 1672 (ν C=O), 1589, 1423 (ν C=C), 1481 (ν N=N), 1392 (ν C-H), 1355 (ν C-N), 1022 (ν_{Inp}, =C-H), 956 (ν_{op} =C-H). Anal. Calcd. for $C_{16}H_{17}N_3O$ (267.33): C, 71.89%; H, 6.41%; and N, 15.72%. Found: C, 71.87%; H, 6.35%; and N, 15.69%.

2.1.3. (E)-3,5-Dimethyl-4-(phenyldiazenyl)aniline (**1c**)

The title compound was obtained as an orange solid, with 74% yield and a melting point of 55–56°C. ^{1}H NMR (400 MHz, $CDCl_3$): δ 7.88–7.82 (m, 2H, CH=CH-CH), 7.54–7.48 (m, 2H, CH=C-N=N), 7.45–7.39 (m, 1H, CH=CH-CH), 6.46 (s, 2H, CH=C-NH$_2$), 3.87 (s, 2H, NH$_2$), 2.51 (s, 6H, CH$_3$). ^{13}C NMR (101 MHz, $CDCl_3$): δ 153.5, 147.4, 142.7, 135.8, 129.6, 128.9, 122.1, 115.3 (Ar), 20.5 (CH$_3$). FTIR (cm^{-1}): 3342 (ν_{as} N-H), 3205 (ν_{si} N-H), 3060 (ν =C-H), 2960, 2912 (ν C-H), 1595, 1477 (ν C=C), 1488 (ν N=N), 1409 (ν C-H), 1326

(ν C-N), 1028 (ν_{Inp}), =C-H), 763 (ν_{op} =C-H). Anal. Calcd. for $C_{14}H_{15}N_3$ (225.30): C, 74.64%; H, 6.71%; and N, 18.65%. Found: C, 74.70%; H, 6.60%; and N, 18.61%.

2.1.4. (E)-3,5-Dimethyl-4-((4-nitrophenyl)diazenyl)aniline (**1d**)

The title compound was obtained as a dark red solid, with 96% yield and a melting point of 159–161 °C. ^{1}H NMR (400 MHz, $CDCl_3$): δ 8.32 (d, *J* = 8.98 Hz, 2H, CH=C-NO_2), 7.87 (d, *J* = 9.01 Hz, 2H, CH=C-N=N), 6.43 (s, 2H, CH=C-NH_2), 4.08 (s, 2H, NH_2), 2.55 (s, 6H, CH_3). ^{13}C NMR (101 MHz, $CDCl_3$): δ 157.1, 149.3, 147.5, 142.1, 138.4, 124.7, 122.4, 115.3 (Ar), 21.4 (CH_3). FTIR (cm^{-1}): 3338 (ν_{as} N-H), 3228 (ν_{si} N-H), 3103 (ν =C-H), 2968, 2914 (ν C-H), 1587 (ν_{as} NO_2), 1585, 1481 (ν C=C), 1508 (ν N=N), 1390 (ν C-H), 1338 (ν NO_2), 1305 (ν C-N), 1026 (ν_{Inp} =C-H), 756 (ν_{op} =C-H). Anal. Calcd. for $C_{14}H_{14}N_4O_2$ (270.29): C, 62.21%; H, 5.22%; and N, 20.73%. Found: C, 62.33%; H, 5.16%; and N, 20.67%.

2.1.5. (E)-4-((4-Methoxyphenyl)diazenyl)-3,5-dimethylaniline (**1e**)

The title compound was obtained as a red solid, with 88% yield and a melting point of 87–88 °C. ^{1}H NMR (400 MHz, $CDCl_3$): δ 7.84 (d, *J* = 8.96 Hz, 2H, CH=C-OCH_3), 7.02 (d, *J* = 8.97 Hz, 2H, CH=C-N=N), 6.45 (s, 2H, CH=C-NH_2), 3.90 (s, 3H, OCH_3), 3.80 (s, 2H, NH_2), 2.46 (s, 6H, CH_3). ^{13}C NMR (101 MHz, $CDCl_3$): δ 161.0, 147.8, 146.8, 142.9, 135.0, 123.7, 115.4, 114.0 (Ar), 55.5 (OCH_3), 20.3 (CH_3). FTIR (cm^{-1}): 3369 (ν_{as} N-H), 3213 (ν_{si} N-H), 3068 (ν =C-H), 2964, 2916 (ν C-H), 1596, 1485 (ν C=C), 1498 (ν N=N), 1431 (ν C-H), 1326 (ν C-N), 1180 (ν_{as}, C-O-C), 1024 (ν_{Inp} =C-H), 1002 (ν_{si}, C-O-C), 750 (ν_{op} =C-H). Anal. Calcd. for $C_{15}H_{17}N_3O$ (255.32): C, 70.56%; H, 6.71%; and N, 16.46%. Found: C, 70.61%; H, 6.66%; and N, 16.32%.

2.1.6. (E)-4-((4-Amino-2,6-dimethylphenyl)diazenyl)benzoic acid (**1f**)

The title compound was obtained as a bright red solid, with 86% yield and a melting point of 167–169 °C. ^{1}H NMR (400 MHz, $CDCl_3$): δ 12.99 (s, 1H, CO_2H), 8.05 (d, *J* = 8.56 Hz, 2H, CH=C-COOH), 7.75 (d, *J* = 8.51 Hz, 2H, CH=C-N=N), 6.37 (s, 2H, CH=C-NH_2), 3.36 (s, 2H, NH_2), 2.46 (s, 6H, CH_3). ^{13}C NMR (101 MHz, $CDCl_3$): δ 167.3 (CO_2H), 155.4, 146.2, 140.1, 135.0, 132.4, 131.0, 122.3, 120.5 (Ar), 20.1 (CH_3). FTIR (cm^{-1}): 3367 (ν_{as} N-H), 3207 (ν_{si} N-H), 3201, 2202 (ν O-H), 3064 (ν =C-H), 2962, 2916 (ν C-H), 1681 (ν C=O), 1596, 1483 (ν C=C), 1498 (ν N=N), 1419 (ν_{Inp} C-O-H), 1398 (ν C-H), 1301 (ν C-N), 1284 (ν_{dim}, C-O), 1028 (ν_{Inp} =C-H), 777 (ν_{op} =C-H). Anal. Calcd. for $C_{15}H_{15}N_3O_2$ (269.30): C, 66.90%; H, 5.61%; and N, 15.60%. Found: C, 66.95%; H, 5.46%; and N, 15.30%.

2.2. General Synthesis of Azo-Maleimides

The synthesis of maleimides (**2a**–**f**) was carried out in two steps. The first step involved an acylation reaction to form the amic acid, resulting from the reaction between the azobenzene-derived amine from 3,5-dimethylaniline and maleic anhydride, using ethyl ether as a solvent at 30 °C. In the second step, without isolating the product, a dehydration reaction was performed to obtain the cyclic amide using acetic anhydride and sodium acetate under reflux.

2.2.1. Step 1: Formation of Amic Acid

In a 50 mL round-bottom flask, 1.5 mmol of the azocompound (**1a**–**f**) was dissolved in 10 mL of ethyl ether. Subsequently, 1.5 mmol of maleic anhydride was added, and the mixture was stirred constantly for two hours at room temperature (30 °C). After the reaction time, an insoluble precipitate formed, which was filtered under vacuum, washed with cold ethyl ether, and dried for use in the next step.

2.2.2. Step 2: Formation of Maleimide

In a round-bottom flask, 3.0 mmol of amic acid was placed along with 3.7 mL of acetic anhydride and 0.01 mol of sodium acetate. The mixture was vigorously stirred and heated to 90 °C until the solid was completely dissolved. Subsequently, the mixture was refluxed

for 3 h. After the reaction time, the mixture was poured into a beaker containing crushed ice and stirred constantly for 30 min. The solid obtained was filtered under vacuum, washed with plenty of distilled water, dried, and recrystallized from ethanol.

2.2.3. (E)-1-(4-((4-Acetylphenyl)diazenyl)-3,5-dimethylphenyl)-1H-pyrrole-2,5-dione (**2a**)

The title compound was obtained as a thin reddish solid, with 60% yield and a melting point of 158–160 °C. ^{1}H NMR (400 MHz, DMSO-d6): δ 8.24–8.15 (m, 2H, CH=C-$COCH_3$), 8.04–7.95 (m, 2H, CH=C-N=N), 7.23 (s, 4H, CH=C-N, CH=CH), 2.67 (s, 3H, $COCH_3$), 2.38 (s, 6H, CH_3). ^{13}C NMR (101 MHz, DMSO-d6): δ ^{13}C 197.95 ($COCH_3$), 170.25 (C=O), 155.02, 149.78, 139.05, 135.29, 132.27, 130.08, 127.63, 122.82 (Ar), 132.21(CH), 27.46 ($COCH_3$), 19.19 (CH_3). FTIR (cm^{-1}): 3105 (ν =C-H), 2964, 2920 (ν C-H), 1714 (ν C=O maleimide) 1681 (ν C=O), 1597, 1475 (ν C=C), 1587 (ν N=N), 1377 (ν C-H), 1398 (ν C-N), 1031 (ν_{Inp} =C-H), 827 (ν_{op} =C-H). Anal. Calcd. for $C_{20}H_{17}N_3O_3$ (347.37): C, 69.15%; H, 4.93%; and N, 12.10%. Found: C, 70.01%; H, 5.20%; and N, 12.02%.

2.2.4. (E)-1-(4-((3-Acetylphenyl)diazenyl)-3,5-dimethylphenyl)-1H-pyrrole-2,5-dione (**2b**)

The title compound was obtained as an orange solid, with 40% yield and a melting point of 140–142 °C. ^{1}H NMR (400 MHz, $CDCl_3$): δ 8.48 (t, *J* = 1.8 Hz, 1H, CH=C-N=N), 8.14 (dt, *J* = 7.7, 1.4 Hz, 1H, CH=C-$COCH_3$), 8.10 (dt, *J* = 7.9, 1.2 Hz, 1H, CH-C-N=N), 7.67 (t, *J* = 7.8 Hz, 1H, CH-CH), 7.17 (t, *J* = 0.7 Hz, 2H, CH=C-N), 6.90 (s, 2H, CH=CH), 2.73 (s, 3H, $COCH_3$), 2.45 (d, *J* = 0.8 Hz, 6H, CH_3). ^{13}C NMR (101 MHz, $CDCl_3$): δ 197.45 ($COCH_3$), 169.44 (C=O), 152.86, 150.14, 138.23, 134.31, 130.93, 130.52, 129.49, 126.57, 126.17, 123.05 (Ar), 132.50 (CH), 26.79 (CH_3), 19.21 (CH_3). FTIR (cm^{-1}): 3091 (ν =C-H), 2977, 2922 (ν C-H), 1714 (ν C=O maleimide) 1681 (ν C=O), 1598, 1498 (ν C=C), 1585 (ν N=N), 1373 (ν C-H), 1394 (ν C-N), 1033 (ν_{Inp} =C-H), 864 (ν_{op} =C-H). Anal. Calcd. for $C_{20}H_{17}N_3O_3$ (347.37): C, 69.15%; H, 4.93%; and N, 12.10%. Found: C, 69.32%; H, 5.10%; and N, 12.19%.

2.2.5. (E)-1-(3,5-Dimethyl-4-(phenyldiazenyl)phenyl)-1H-pyrrole-2,5-dione (**2c**)

The title compound was obtained as an orange solid, with 86% yield and a melting point of 185–186 °C. ^{1}H NMR (400 MHz, $CDCl_3$): δ 7.89 (dd, *J* = 7.7, 2.1 Hz, 2H, CH=CH-CH), 7.64 (m, 1H, CH=C-N=N), 7.63–7.61 (m, 2H, 1H, CH=CH-CH), 7.22 (s, 2H, CH=C-N), 7.19 (s, 2H, CH=CH), 2.33 (s, 6H, CH_3). ^{13}C NMR (101 MHz, $CDCl_3$): δ 170.3 (C=O), 152.8, 150.2, 135.3, 131.6, 131.5, 130.0, 127.6, 122.7 (Ar), 132.2 (C=C) 18.9 (CH_3). FTIR (cm^{-1}): 3101 (ν =C-H), 2977, 2925 (ν C-H), 1712 (ν C=O), 1596, 1477 (ν C=C), 1490 (ν N=N), 1398 (ν C-H), 1377 (ν C-N), 1029 (ν_{Inp} =C-H), 763 (ν_{op} =C-H). Anal. Calcd. for $C_{18}H_{15}N_3O_2$ (305.34): C, 70.81%; H, 4.95%; and N, 13.76%. Found: C, 70.51%; H, 4.80%; and N, 13.82%.

2.2.6. (E)-1-(3,5-Dimethyl-4-((4-nitrophenyl)diazenyl)phenyl)-1H-pyrrole-2,5-dione (**2d**)

The title compound was obtained as a dark red solid, with 94% yield and a melting point of 261–262 °C. ^{1}H NMR (400 MHz, $CDCl_3$): δ 8.46 (d, *J* = 8.95 Hz, 2H, CH=C-NO_2), 8.09 (d, *J* = 8.95 Hz, 2H, CH=C-N=N), 7.25 (s, 2H, CH=C-N), 7.23 (s, 2H, CH=CH), 2.43 (s, 6H, CH_3). ^{13}C NMR (101 MHz, $CDCl_3$): 170.2 (C=O), 155.8, 149.3, 149.1, 135.3, 132.8, 127.7, 125.6, 123.7 (Ar), 132.9 (C=C), 19.4 (CH_3). FTIR (cm^{-1}): 3103 (ν =C-H), 2974, 2927 (ν C-H), 1714 (ν C=O), 1608 (ν_{as} NO_2), 1589, 1492 (ν C=C), 1517 (ν N=N), 1396 (ν C-H), 1375 (ν C-N), 1342 (ν_{si} NO_2), 1031 (ν_{Inp} =C-H), 754 (ν_{op} =C-H). Anal. Calcd. for $C_{18}H_{14}N_4O_4$ (350.33): C, 61.71%; H, 4.03%; and N, 15.99%. Found: C, 61.52%; H, 4.18%; and N, 15.82%.

2.2.7. (E)-1-(4-((4-Methoxyphenyl)diazenyl)-3,5-dimethylphenyl)-1H-pyrrole-2,5-dione (**2e**)

The title compound was obtained as a red solid, with 88% yield and a melting point of 183–184 °C. ^{1}H NMR (400 MHz, $CDCl_3$): δ 7.89 (d, *J* = 6.96 Hz, 2H, CH=C-OCH_3), 7.21 (s, 2H, CH=C-N=N), 7.17 (s, 2H, CH=C-N), 7.15 (s, 2H, CH=CH), 3.88 (s, 3H, OCH_3), 2.29 (s, 6H, CH_3). ^{13}C NMR (101 MHz, $CDCl_3$): δ 170.4 (C=O), 162.7, 150.4, 147.0, 135.2, 131.00, 127.5, 124.7, 115.1 (Ar), 131.2 (C=C), 56.2 (OCH_3), 18.8 (CH_3). FTIR (cm^{-1}): 3089 (ν =C-H), 2974, 2920 (ν C-H), 1708 (ν C=O), 1595, 1483 (ν C=C), 1498 (ν N=N), 1396 (ν C-H), 1371 (ν

C-N), 1184 (ν_{as} C-O-C), 1026 (ν_{Inp} =C-H), 985 (ν_{si} C-O-C), 767 (ν_{op} =C-H). Anal. Calcd. for $C_{19}H_{17}N_3O_3$ (335.36): C, 68.05%; H, 5.11%; and N, 12.53%. Found: C, 67.98%; H, 5.27%; and N, 12.25%.

2.2.7.1. (E)-4-((4-(2,5-Dioxo-2,5-dihihydro-1H-pyrro-1-yl)-2,6-dimethylphenyl)diazinyl) benzoic acid (**2f**)

The title compound was obtained as a red bright solid, with 84% yield and a melting point of 255–256 °C. ^{1}H NMR (400 MHz, $CDCl_3$): δ 13.23 (s,1H, CO_2H), 8.17 (d, *J* = 8.49 Hz, 2H, CH=C-COOH), 7.97 (d, *J* = 8.52 Hz, 2H, CH=C-N=N), 7.23 (s, 2H, CH=C-N), 7.22 (s, 2H, CH=CH), 2.38 (s, 6H, CH_3). ^{13}C NMR (101 MHz, $CDCl_3$): δ 170.3 (C=O), 167.2 (CO_2H), 155.0, 149.8, 135.3, 134.3, 133.6, 131.1, 127.6, 122.7 (Ar), 132.2 (C=C) 19.2 (CH_3). FTIR (cm^{-1}): 3145–2368 (ν O-H), 3101 (ν =C-H), 2979, 2922 (ν C-H), 1714 (ν C=O maleimide), 1681 (ν C=O COOH), 1596, 1471 (ν C=C), 1502 (ν N=N), 1423 (ν_{Inp} C-O-H), 1398 (ν C-H), 1375 (ν C-N), 1288 (ν C-O), 1024 (ν =C-H), 775 (ν_{op} =C-H). Anal. Calcd. for $C_{19}H_{15}N_3O_4$ (349.35): C, 65.32%; H, 4.33%; and N, 12.03%. Found: C, 65.10 %; H, 4.51%; and N, 12.22%.

2.3. General Procedure of Azo-Oxanorbornenes

The synthesis of azo-oxanorbornenes (**3a**–**f**) was performed via a Dies–Alder cycloaddition reaction. In a round-bottom flask, 5.0 mmol of **2a**–**f** was dissolved in 10 mL of acetonitrile at 70 °C. Subsequently, the solution was cooled to 5 °C using an ice bath. Afterward, 3 mL of furan was added, and the reaction mixture was stirred constantly for 72 h. The progress of the reaction was monitored by thin-layer chromatography (TLC) using a TLC silica gel 60 F_{254} plastic sheet and ethyl acetate/hexane 50/50 as the eluent at 30 °C. After the reaction time, the solvent was evaporated, and the adduct was washed with cold diethyl ether and recrystallized from ethanol.

2.3.1. (E)-2-(4-((4-Acetylphenyl)diazenyl)-3,5-dimethylphenyl)-3a,4,7,7a-tetrahydro-1H-4,7-epoxyisoindole-1,3(2H)-dione (**3a**)

The title compound was obtained as a thin reddish solid, with 70% yield and a melting point of 160–162 °C. ^{1}H NMR (400 MHz, DMSO-d6): δ ^{1}H NMR (400 MHz, DMSO) δ 8.23–8.15 (m, 2H, CH=C-$COCH_3$), 8.03–7.90 (m, 2H, CH=C-N=N), 7.11–7.04 (m, 2H, CH=C-N), 6.63 (t, *J* = 0.9 Hz, 2H, CH=CH), 5.28 (t, *J* = 1.0 Hz, 2H, Bridgehead), 3.12 (s, 2H, CH-$CH_{maleimide}$), 2.67 (s, 3H, $COCH_3$), 2.36 (s, 6H, CH_3). ^{13}C NMR (101 MHz, DMSO-d6): δ 197.97 ($COCH_3$), 176.11 (C=O), 154.94, 150.48, 139.11, 132.60, 132.10, 130.10, 127.83, 122.86 (Ar), 137.13 (C=C), 81.29 (CH), 48.04 (CH), 27.49 (CH_3), 18.95 (CH_3). FTIR (cm^{-1}): 3107 (ν =C-H), 2964, 2925 (ν C-H), 1714 (ν C=O maleimide) 1689 (ν C=O), 1593, 1425 (ν C=C), 1471 (ν N=N), 1380 (ν C-H), 1282 (ν C-N), 1184 (ν_{as} C-O-C), 1070 (ν_{Inp} =C-H), 1014 (ν_{si} C-O-C), 960 (ν_{op} =C-H). Anal. Calcd. for $C_{24}H_{21}N_3O_4$ (415.45): C, 69.39%; H, 5.10%; and N, 10.11%.Found: C, 69.61%; H, 5.00%; and N, 10.22%.

2.3.2. (E)-2-(4-((3-Acetylphenyl)diazenyl)-3,5-dimethylphenyl)-3a,4,7,7a-tetrahydro-1H-4,7-epoxyisoindole-1,3(2H)-dione (**3b**)

The title compound was obtained as an orange solid, with 40% yield and a melting point of 140–142 °C. ^{1}H NMR (400 MHz, DMSO-d6): δ 8.39 (t, *J* = 1.8 Hz, 1H, CH=C-N=N), 8.20 (ddd, *J* = 7.7, 1.7, 1.1 Hz, 1H, CH=C-$COCH_3$), 8.13 (ddd, *J* = 7.9, 2.1, 1.1 Hz, 1H, CH-C-N=N), 7.79 (t, *J* = 7.8 Hz, 1H, CH-CH), 7.08 (t, *J* = 0.7 Hz, 2H, CH=C-N), 6.66–6.61 (m, 2H, CH=CH), 5.28 (t, *J* = 1.0 Hz, 2H, Bridgehead), 3.12 (s, 2H, CH-$CH_{maleimide}$), 2.70 (s, 3H, $COCH_3$), 2.35 (s, 6H, CH_3). ^{13}C NMR (101 MHz, DMSO-d6): δ 197.97 ($COCH_3$), 176.13 (C=O), 154.62, 152.77, 138.55, 131.82, 130.57, 127.77, 126.31, 122.58, 120.44 (Ar), 137.13 (C=C), 81.29 (CH), 48.03 (CH), 27.45 (CH_3), 18.85 (CH_3). FTIR (cm^{-1}): 3091 (ν =C-H), 2966, 2922 (ν C-H), 1705 (ν C=O maleimide) 1676 (ν C=O), 1598, 1463 (ν C=C), 1500 (ν N=N), 1421 (ν C-H), 1384 (ν C-N), 1191 (ν_{as} C-O-C), 1105 (ν_{Inp} =C-H), 1010 (ν_{si} C-O-C), 914 (ν_{op} =C-H). Anal. Calcd. for $C_{24}H_{21}N_3O_4$ (415.45): C, 69.39%; H, 5.10%; and N, 10.11%. Found: C, 69.77%; H, 5.27%; and N, 10.19%.

2.3.3. (E)-2-(3,5-Dimethyl-4-(phenyldiazenyl)phenyl)-3a,4,7,7a-tetrahydro-1H-4,7-epoxyisoindole-1,3(2H)-dione (**3c**)

The title compound was obtained as an orange solid, with 97% yield and a melting point of 127–129 °C. ^{1}H NMR (400 MHz, $CDCl_3$): δ 7.90 (dd, *J* = 7.58, 2.19 Hz, 2H, CH=CH-CH), 7.64 (s, 1H, CH=C-N=N), 7.62 (s, 2H, CH=CH-CH), 7.05 (s, 2H, CH=C-N), 6.63 (s, 2H, CH=CH), 5.28 (s, 2H, Bridgehead), 3.11 (s, 2H, CH-$CH_{maleimide}$), 2.30 (s, 6H, CH_3). ^{13}C NMR (101 MHz, $CDCl_3$): δ 176.1(C=O), 152.7, 150.8, 132.2, 131.9, 131.4, 129.9, 127.6, 122.7 (Ar), 137.1 (C=C) 81.2 (CH), 48.0 (CH), 18.6 (CH_3). FTIR (cm^{-1}): 3068 (ν =C-H), 2977, 2920 (ν C-H), 1710 (ν C=O), 1596, 1477 (ν C=C), 1485 (ν N=N), 1380 (ν C-H), 1286 (ν C-N), 1188 (ν_{as} C-O-C), 1014 (ν_{inp} =C-H), 1002 (ν_{si} C-O-C), 767 (ν_{op} =C-H). Anal. Calcd. for $C_{22}H_{19}N_3O_3$ (373.41): C, 70.76%; H, 5.13%; and N, 11.25%. Found: C, 70.52%; H, 5.42%; and N, 11.54%.

2.3.4. (E)-2-(3,5-Dimethyl-4-((4-nitrophenyl)diazenyl)phenyl)-3a,4,7,7a-tetrahydro-1H-4,7-epoxyisoindole-1,3(2H)-dione (**3d**)

The title compound was obtained as a dark red solid, with 98% yield and a melting point of 130–132 °C. ^{1}H NMR (400 MHz, $CDCl_3$): δ 8.45 (d, *J* = 8.27 Hz, 2H, CH=C-NO_2), 8.08 (d, *J* = 8.41 Hz, 2H, CH=C-N=N), 7.10 (s, 2H, CH=C-N), 6.63 (s, 2H, CH=CH), 5.27 (s, 2H, Bridgehead), 3.12 (s, 2H, CH-$CH_{maleimide}$), 2.38 (s, 6H, CH_3). ^{13}C NMR (101 MHz, $CDCl_3$): δ 176.0 (C=O), 155.7, 150.0, 149.1, 133.1, 132.7, 127.9, 125.5, 123.7 (Ar), 137.1 (C=C), 81.3 (CH), 48.0 (CH), 19.1 (CH_3). FTIR (cm^{-1}): 3107 (ν =C-H), 2960, 2922 (ν C-H), 1708 (ν C=O), 1602 (ν_{as} NO2), 1595, 1492 (ν C=C), 1519 (ν N=N), 1373 (ν C-H), 1342 (ν_{si} NO_2), 1317 (ν C-N), 1188 (ν_{as} C-O-C), 1018 (ν_{Inp} =C-H), 1010 (ν_{si} C-O-C), 757 (ν_{op} =C-H). Anal. Calcd. for $C_{22}H_{18}N_4O_5$ (418.41): C, 63.15%; H, 4.34%; and N, 13.39%. Found: C, 63.41%; H, 4.65%; and N, 13.24%.

2.3.5. (E)-2-(4-((4-Methoxyphenyl)diazenyl)-3,5-dimethylphenyl)-3a,4,7,7a-tetrahydro-1H-4,7-epoxyisoindole-1,3(2H)-dione (**3e**)

The title compound was obtained as an orange solid, with 96% yield and a melting point of 180–182 °C. ^{1}H NMR (400 MHz, $CDCl_3$): δ 7.89 (d, *J* = 8.88 Hz, 2H, CH=C-OCH_3), 7.16 (d, *J* = 8.98 Hz, 2H, CH=C-N=N), 7.02 (s, 2H, CH=C-N), 6.63 (s, 2H, CH=CH), 5.27 (s, 2H, Bridgehead), 3.88 (s, 3H, OCH_3), 3.10 (s, 2H, CH-$CH_{maleimide}$), 2.27 (s, 6H, CH_3). ^{13}C NMR (101 MHz, $CDCl_3$): δ 176.1 (C=O), 162.8, 151.0, 147.0, 131.5, 131.1, 127.5, 124.7, 115.1 (Ar), 137.1 (C=C), 81.3 (CH), 56.2 (OCH_3), 47.9 (CH), 18.6 (CH_3). FTIR (cm^{-1}): 3078 (ν =C-H), 2970, 2920 (ν C-H), 1712 (ν C=O), 1596, 1479 (ν C=C), 1502 (ν N=N), 1375 (ν C-H), 1313 (ν C-N), 1193 (ν_{as} C-O-C), 1029 (ν_{Inp} =C-H), 1012 (ν_{si} C-O-C), 752 (ν_{op} =C-H). Anal. Calcd. for $C_{23}H_{21}N_3O_4$ (403.44): C, 68.47%; H, 5.25%; and N, 10.42%. Found: C, 68.64%; H, 5.12%; and N, 10.39%.

2.3.6. (E)-4-((4-(1,3-Dioxo-2,3,3a,4,7,7a-tetrahydro-1H-4,7-epoxyisoindol-2(3H)-yl)-2,6-dimethylphenyl)diazenyl) benzoic acid (**3f**)

The title compound was obtained as a red bright solid, with 90% yield and a melting point of 286–288 °C. ^{1}H NMR (400 MHz, $CDCl_3$): δ 8.17 (d, *J* = 8.43 Hz, 2H, CH=C-COOH), 7.94 (d, *J* = 8.45 Hz, 2H, CH=C-N=N), 7.08 (s, 2H, CH=C-N), 6.63 (s, 2H, CH=CH), 5.28 (s, 2H, Bridgehead), 3.12 (s, 2H, CH-$CH_{maleimide}$), 2.35 (s, 6H, CH_3). ^{13}C NMR (101 MHz, $CDCl_3$): δ: 176.0 (C=O), 167.6 (CO_2H), 154.6, 150.5, 134.1, 132.4, 131.9, 131.0, 127.7, 122.5 (Ar), 137.1 (C=C), 81.3 (CH), 48.0 (CH), 18.8 (CH_3). FTIR (cm^{-1}): 3163–2360 (ν O-H), 3078 (ν =C-H), 2981, 2923 (ν C-H), 1706 (ν C=O maleimide), 1687 (ν C=O (CO_2H)), 1598, 1481 (ν C=C), 1500 (ν N=N), 1421 (ν_{inp} C-O-H), 1377 (ν C-H), 1303 (ν C-N), 1286 (ν C-O), 1188 (ν_{as} C-O-C), 1024 (ν =C-H), 1012 (ν_{si} C-O-C), 777 (ν_{op} =C-H). Anal. Calcd. for $C_{23}H_{19}N_3O_5$ (417.42): C, 66.18%; H, 4.59%; and N, 10.07%. Found: C, 66.21%; H, 4.50%; and N, 10.00%.

2.4. Electrochemical Analysis

Voltametric measurements were conducted using a Voltalab PGZ100 potentiostat/galvanostat (Hach, Lyon, France). A typical three-electrode cell was employed: a

glassy carbon (GC) electrode with a diameter of 3 mm as the working electrode, a platinum wire as the counter electrode, and a 3.0 M Ag/AgCl electrode as the reference. All potentials were reported versus this reference electrode. The GC electrode was mechanically polished using an alumina slurry with particle sizes of 1 µm, 0.3 µm, and 0.05 µm, in that order, for 3 min each on a polishing pad. The electrode was then sonicated in distilled water for 5 min, followed by sonication in ethanol for 5 min, before the analyses began. Cyclic voltammetry was performed in an acetonitrile (MeCN) solution containing 0.1 M tetrabutylammonium tetrafluoroborate ($TBABF_4^-$, Sigma-Aldrich, Burlington, MA, USA) as the supporting electrolyte. All measurements were taken at a scan rate of 100 mV/s, starting from the open-circuit potential (OCP), either towards the anodic or cathodic region.

2.5. Characterization of Compounds

The FTIR spectra of all compounds were obtained in a Bruker Tensor-27 spectrophotometer (Bruker corporation, Billerica, MA, USA) equipped with an attenuated total reflectance (ATR) system of 16 scans, with a spectral range of 600–4000 cm^{-1} and a resolution of 4 cm^{-1}. The ^1H and ^{13}C NMR spectra of all compounds were recorded on a Bruker 400 advance III spectrometer (^1H = 400 MHz and ^{13}C = 101 MHz) (Bruker corporation, Billerica, USA) at room temperature (25 °C) using DMSO-d_6 (Sigma-Aldrich, Burlington, MA, USA) and $CDCl_3$ (Sigma-Aldrich, Burlington, MA, USA) as the solvent. The processing of NMR spectra was performed using the *MestReNova* Software (version 14.2.1-27684; Mestrelab Research, 2021). Elemental analysis was performed on a Thermo Scientific/Flash 2000 (Thermo Fisher Scientific, Waltham, MA, USA). The melting points were determined using an Electrothermal MEL-TEMP apparatus (Electrothermal, Chicago, IL, USA) in open capillary tubes, which were not corrected.

3. Results and Discussion

*3.1. Synthesis and Characterization of Azocompounds (***1a–3f***)*

In the present work, we describe the synthesis of new *exo-N*-azobenzene oxa-norbornene dicarboximides **3a–f** via a Dies–Alder reaction between furan and azobenzene maleimide derivatives **2a–f**. These *N*-substituted maleimide compounds were prepared by reacting 4-aminoazobenzene with maleic anhydride in a two-step synthesis. The synthesis of six aminoazobenzene derivatives was carried out via classical diazotization-coupling reaction, all derived from 3,5-dimethylaniline as the coupling agent because we observed that this amine provided good yields (up to 70%) of the amino diazo compound (Scheme 1). Since 3,5-dimethylaniline could undergo a diazotization reaction due to the slight excess of nitrosonium ion, it was necessary to consider measures to avoid the formation of undesired azocompounds. Once the diazotization time had elapsed, it was important to neutralize completely the nitrosonium ion with urea before adding the coupling agent.

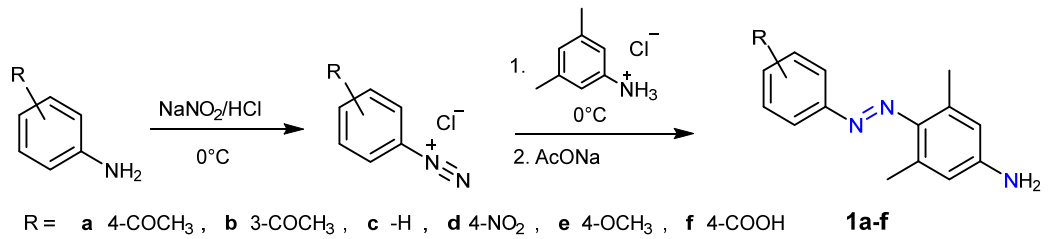

Scheme 1. Synthesis of aminoazobenzenes via diazotization-coupling reaction.

The structures of the synthesized amino diazo intermediates **1a–f** were confirmed by IR, ^1H, and ^{13}C NMR spectroscopy. The IR spectra of the aminoazobenzene compounds (selected frequencies are listed in Table 1) show an absorption band between 1487 and 1508 cm^{-1} which corresponds to the azo group (-N=N-), indicating that the diazotization coupling reaction has been carried out, along with symmetric and antisymmetric absorp-

tion bands of the N-H group around 3228–3205 cm^{-1} and 3369–3324 cm^{-1}, respectively (Figure 1). The aminoazobenzenes **1a**, **1b**, and **1f** show an absorption band at frequencies 1668, 1673, and 1681 cm^{-1}, respectively, corresponding to the carbonyl group (C=O); meanwhile, compound **1e** shows an absorption band at 1002 cm^{-1}, corresponding to the C-O frequency of the ether group (Ar-OCH_3). The IR spectrum of compound **1d** exhibits the typical absorption bands corresponding to symmetric and antisymmetric stretching vibrations of the nitro groups (NO_2) at 1338 and 1597 cm^{-1}, respectively. Finally, compound **1f** shows a broad absorption band at 3201 cm^{-1} corresponding to the -OH of the carboxylic acid group. The ^{1}H NMR spectra of compounds **1a**–**f** were analyzed, and the proton chemical shifts were determined based on the multiplicity patterns of their resonances. The ^{1}H NMR spectra of aminoazobenzenes display three common signals belonging to the coupling agent: the -NH_2 protons show a single signal at 3.90 ppm (2H), the aromatic protons appear as a single signal around δ = 6.4 ppm (2H), and the -CH_3 group appears around δ = 2.50 ppm (6H). The aromatic protons from the diazonium salt fragment show classic AA'XX' multiplet patterns in compounds **1a** and **1c**–**f**, around δ = 7.00–8.30 ppm (4H). The chemical shifts of these protons depend on the substituent used on the benzene ring. Compounds **1a** and **1b** exhibit a signal around δ = 2.7 ppm (3H) corresponding to a methyl group attached to a carbonyl ketone. In addition, the ^{13}C NMR spectra of the synthesized aminoazobenzenes show eight signals within δ = 114–161 ppm, corresponding to the aromatic carbons of both the diazotized arylamines and the coupling agent. Compounds **1a**, **1b**, and **1f** display signals corresponding to a carbonyl group at δ = 197.7 ppm and δ = 167.3 ppm, respectively. Compound **1e** shows a signal at δ = 55.5 ppm, corresponding to the methoxy group. All aminoazobenzenes show a signal around δ = 20–22 ppm corresponding to the 3,5-dimethylaniline fragment, and, finally, compounds **1a** and **1b** show a signal at δ = 27 ppm due to acetophenone.

Table 1. Selected infrared spectral data and physical properties of the aminoazobenzenes.

Compound	Yield %	M.m (g/mol)	Molecular Formula	Color	m.p. °C	ν (cm^{-1})		
						-N=N-	N-H	C=O
1a	81	267.1	$C_{16}H_{17}N_3O$	reddish	100–102	1487	3209, 3357	1668
1b	78	267.1	$C_{16}H_{17}N_3O$	orange	98–100	1481	3348, 3444	1672
1c	74	225.3	$C_{14}H_{15}N_3$	orange	55–56	1488	3205, 3342	-
1d	96	270.3	$C_{14}H_{14}N_4O_2$	dark red	159–161	1508	3228, 3338	-
1e	88	255.3	$C_{15}H_{17}N_3O$	red	87–88	1498	3213, 3369	-
1f	86	269.3	$C_{15}H_{15}N_3O_2$	bright red	167–169	1498	3207, 3367	1681

Maleic anhydride reacts readily with aminoazobenzenes to form the corresponding amic acids, which are then cyclized to maleimides using acetic anhydride as a dehydrating agent (Scheme 2).

The structures of azobenzene maleimide derivatives **2a**–**f** were confirmed by IR, ^{1}H, and ^{13}C NMR spectroscopy. The IR spectra of compounds **2a**–**f** exhibited typical absorption bands due to symmetric and antisymmetric stretching vibrations of the carbonyl groups, at 1708–1715 cm^{-1} and 1769–1780 cm^{-1}, respectively. Additionally, the absence of the characteristic absorption band for the -NH_2 group in the IR spectroscopic analysis of maleimides suggested the occurrence of an acylation reaction. The ^{1}H NMR spectra of the azobenzene maleimide derivatives **2a**–**f** were similar to those of their parent aminoazobenzenes. A new singlet signal corresponding to olefinic protons appeared around δ = 6.90–7.23 ppm. Additionally, the signal around δ = 3.9 ppm corresponding to the amine group disappeared due to the acylation reaction with maleic anhydride, as shown for the series of compounds **1a**–**3a** in Figure 2. The ^{13}C NMR spectra of compounds **2a**–**f** display two new signals corresponding to the maleimide fragment: one downfield, around δ = 170 ppm, corresponding to the carbonyl group of the maleimide, and another around δ = 131–132 ppm, corresponding to olefinic carbon.

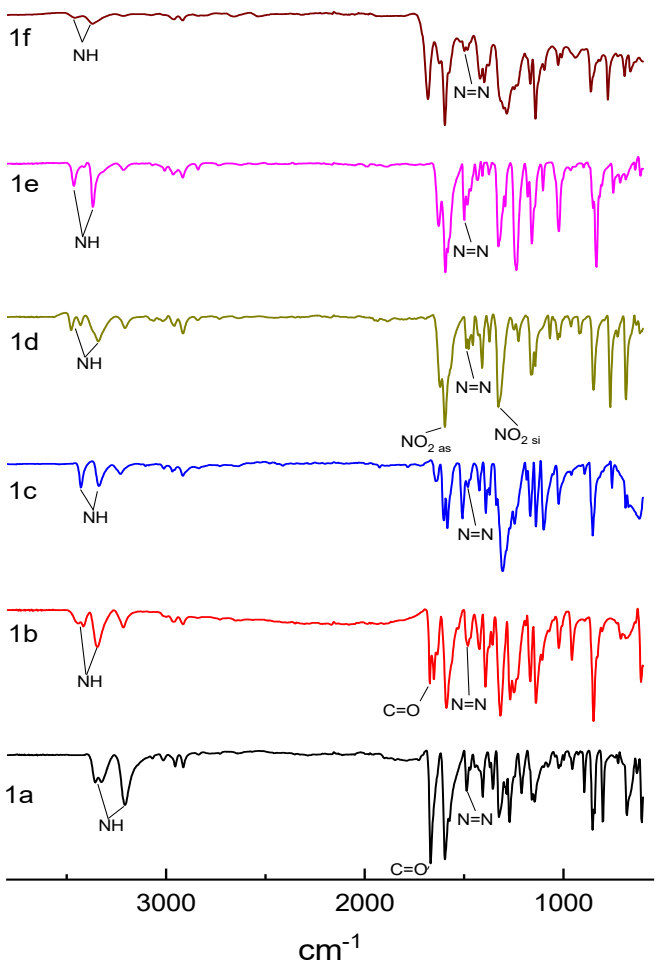

Figure 1. IR spectra of aminoazobenzenes.

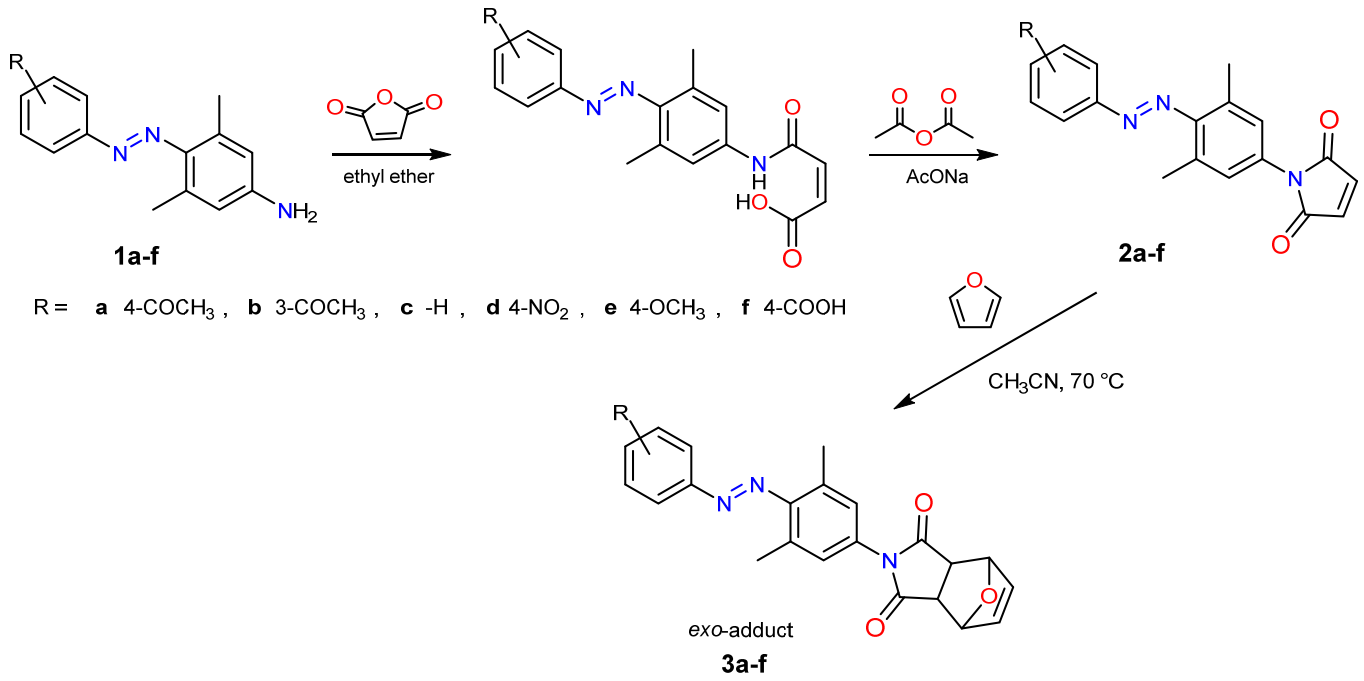

Scheme 2. Synthesis of azobenzene maleimides and their Dies–Alder cycloaddition reaction.

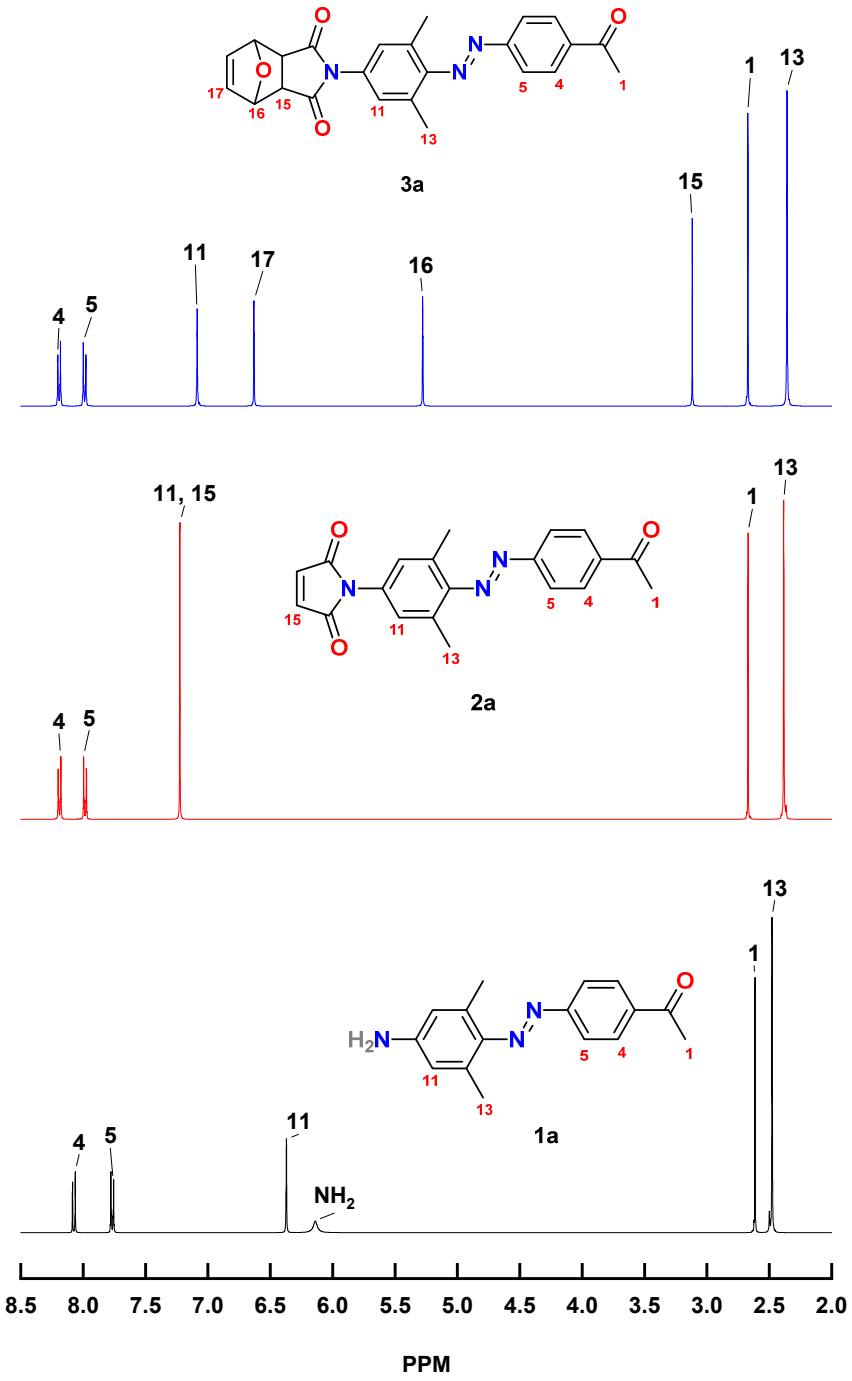

Figure 2. Assignment of ^{1}H NMR peaks of compounds **1a**, **2a**, and **3a**.

The azobenzene maleimide derivatives **2a–f** were used as dienophiles in the Dies–Alder cycloaddition reaction with furan (Scheme 2), similar to the cycloadditions with furan derivatives reported by Mitrasov [65] and Daeffler [66]. The structure of the resulting adducts **3a–f** were confirmed by IR, ^{1}H, and ^{13}C NMR spectroscopy. The IR spectra of compounds **3a–f** do not show significant signals that differentiate them from azobenzene maleimide derivatives. The ^{1}H NMR spectra of compounds **3a–f** display two new signals from the oxanorbornene fragment formed by Dies–Alder cycloaddition: a singlet at δ = 5.3 ppm corresponding to the bridgehead protons, and another singlet at δ = 3.10 ppm corresponding to the protons α to the carbonyl group. The Dies–Alder adducts of furan and maleic anhydride or maleimide derivatives corresponded, predominantly, to the *exo* isomer [67]. The *exo* isomer adducts obtained in this work were

confirmed by the absence of the spin–spin coupling constants between the bridgehead proton with α protons [68]. The signal from the C=C double bond in compounds **3a–f** was no longer de-shielded by the carbonyl groups in the double bond of maleimides **2a–f**, resulting in the signal being shifted to a higher field (Figure 2). The ^{13}C NMR spectra of the adducts **3a–f** display two new signals from the oxanorbornene fragment: the bridgehead carbon and the α carbon, around δ = 81 ppm and δ = 48 ppm, respectively.

3.2. Electrochemical Study of the Redox Reactions

The electrochemical study of the redox reactions of the new *exo-N*-azobenzene oxanorbornene dicarboximides **3a–f**, using cyclic voltammetry, began with the analysis of the raw materials used in the synthesis of the compounds under study. In this regard, Figure 3 shows the cyclic voltammograms (CV) of MeCN (blue line), MeCN with the electrolyte (red line), and MeCN with the supporting electrolyte after the solution was bubbled with N_2 for 10 min, maintaining the N_2 atmosphere during the experiment. In the CVs of MeCN and MeCN + $TBABF_4^-$, a reduction current peak can be observed between −0.75 V (peak A1, red line) and −1.1 V (peak A2, blue line). Similarly, an oxidation peak is observed in these same CVs between 0.9 V (peak A3, red line) and 1.2 V (peak A4, blue line). This latter peak was observed when the reduction peak was generated, indicating the reverse reaction of the reduction. When the solution was bubbled with N_2, the reduction peak disappeared, suggesting that it was due to dissolved oxygen in the solution [69].

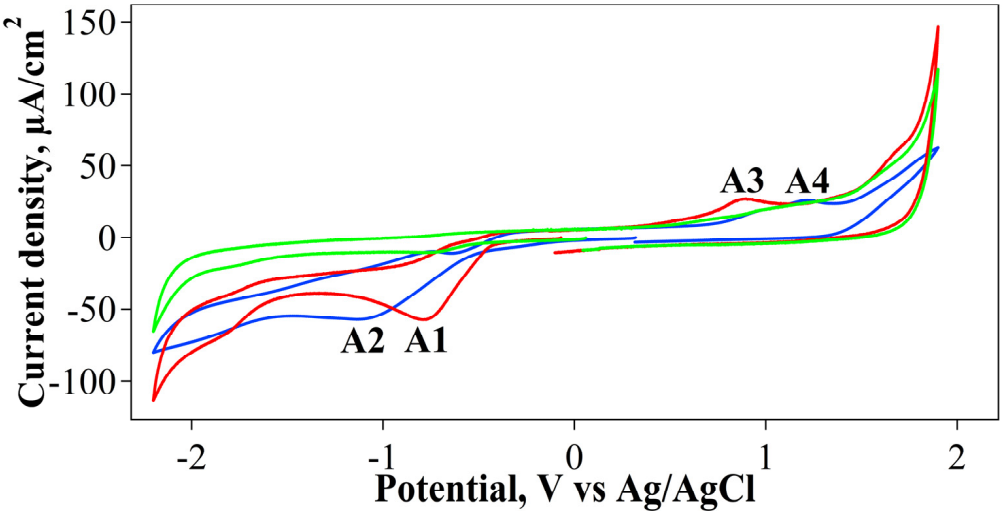

Figure 3. CVs from MeCN (blue line), MeCN + $TBABF_4^-$ (red line), and MeCN + $TBABF_4^-$ bubbled with N_2 (green line).

In Figure 4, the CVs of 4-aminoacetophenone (**1a**) are shown. The formation of the same current peaks (Figure 4, peaks A1 and A2; the notation for A1 and A2 from Figure 3 is repeated here because it refers to the same redox reactions) is evident regardless of the starting point of the voltammogram, whether towards the cathodic region (blue line) or the anodic region (red line), except for a small oxidation peak observed at approximately 0.5 V (peak B) which is only generated when the reduction peak occurs at approximately −1 V, indicating the reverse reaction of that reduction. These current peaks may be due to the presence of oxygen in the solution, as they are obtained at potentials similar to those shown in Figure 3.

Sun et al. [70] reported voltammograms with a similar behavior. The authors mention that the oxidation peak appearing at approximately 1.2 V (Figure 4, peak C) is due to the oxidation of the ketone, forming a ketone radical cation (ketone$^{\bullet+}$). In comparison, the reduction peak C2 at approximately −2 V is attributed to the reduction of the neutral ketone to a ketone radical anion (ketone$^{\bullet-}$). The small reduction peak C1 observed at approximately 0.3 V is due to the reduction of the ketone radical cation (ketone$^{\bullet+}$). This

current peak only appears when the oxidation peak of the ketone (peak C, at approximately 1.2 V) is present.

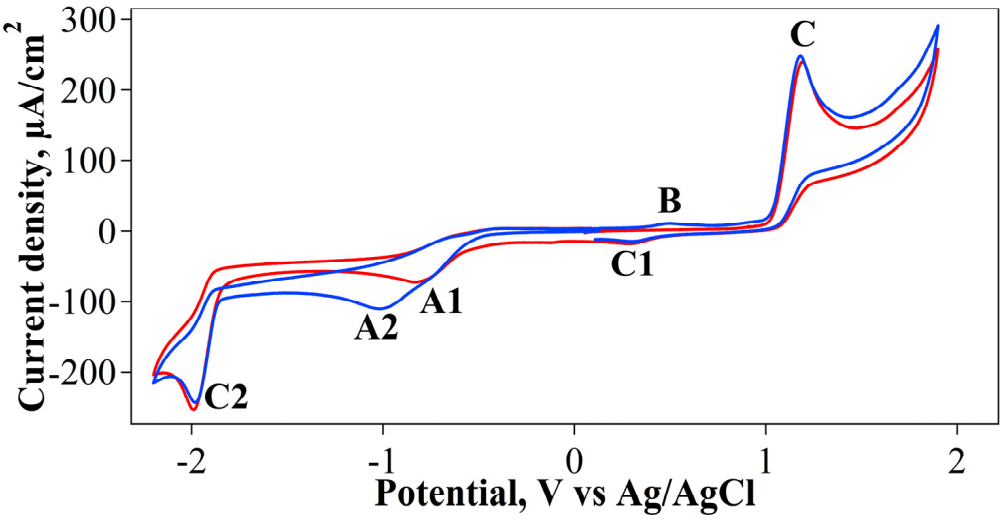

Figure 4. CV of 4-aminoacetophenone in an MeCN + 0.1 M TBABF4^{-} solution. Voltammograms start at the OCP towards the cathodic region (blue line) and anodic region (red line).

In Figure 5, the CVs of 3,5-dimethylaniline towards the cathodic region (blue line) and the anodic region (red line) are shown, with the same peaks observed in both voltammograms, except for the reduction peak at 0 V (peak D3, red line), which is generated when the two oxidation peaks at 0.8 V (peak D1) and 1 V (peak D2) appear, indicating the reverse reaction of that oxidation.

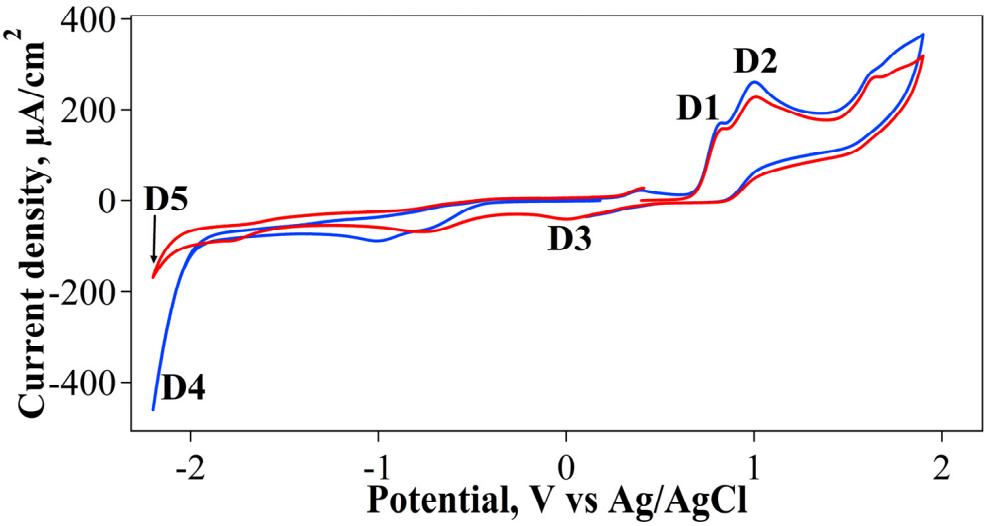

Figure 5. CV of the 3,5-dimethylaniline in an MeCN + 0.1 M TBABF$_4$$^{-}$ solution. The voltammograms start at the OCP towards the cathodic region (blue line) and anodic region (red line).

The oxidation peaks at 0.8 V and 1V (Figure 5) are due to the oxidation of the amine, with the first peak resulting from the loss of one electron, generating the monocation radical $H_2N^{\bullet+}$ and subsequently losing another electron, forming the dication radical H_2N^{++}. This radical reacts with a neutral molecule of 3,5-dimethylaniline to form 3,3′,5,5′-tetramethylhydrazobenzene, which instantly oxidizes to give 3,3′,5,5′-tetramethylazobenzene, analogous to the reaction mechanism proposed by Sharma et al. [71]. The reduction peak at −2.2 V is larger when the CV starts towards the cathodic region (peak D4) than when it starts towards the anodic region

(peak D5). This may be due to the formation of a poorly conductive polymeric layer on the electrode surface during the oxidation of 3,5-dimethylaniline.

In Figure 6, the CV of oxa-norbornene-5,6-dicarboxylic anhydride is presented. The same voltammogram was observed when N_2 was bubbled into the solution, ruling out any redox process caused by dissolved oxygen. Therefore, the reduction peaks generated at approximately −0.8 V (peak E1) may be due to the reduction of the carbonyl groups present in the molecule. When five cycles were scanned instead of just one (supporting information) over a voltage range of −2 V to 1.9 V, these carbonyl reduction peaks decreased with each cycle. However, when five cycles were scanned within a voltage range of −2 V to 0.5 V (a range where the oxidation peak E3 at approximately 1.6 V did not appear), these peaks increased with each cycle. This behavior may indicate that, in the aforementioned oxidative process, a non-conductive polymer is being generated, which could also cause the reduction peak E2 (red line) at −2.2 V to decrease when the CV starts toward the anodic region. This process may be similar to that proposed by Akbulut and Hacioglu [72] for the reduction of maleic anhydride; however, in this case, it would involve polymerization via the formation of carbocations through the oxidation of the double bond.

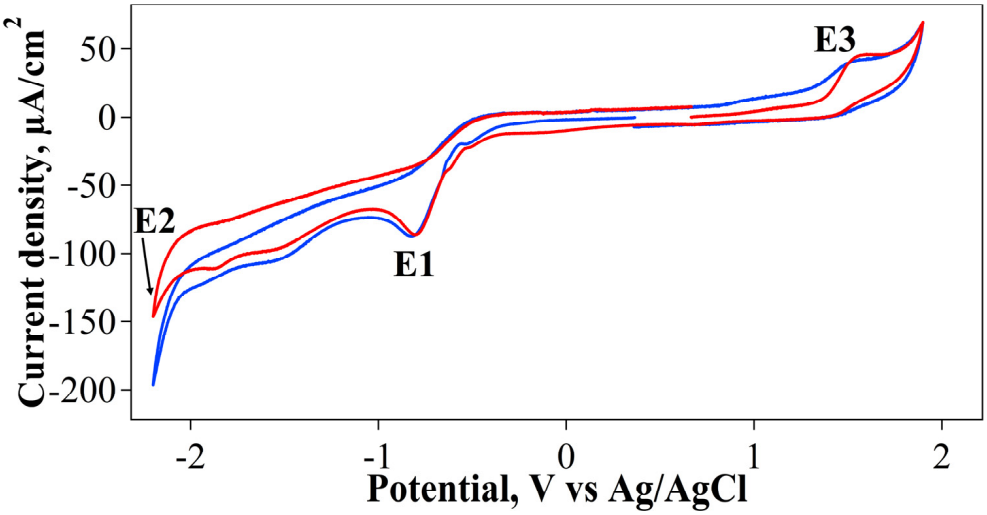

Figure 6. CV of the oxa-norbornene-5,6-dicarboxylic anhydride in an MeCN + 0.1 M $TBABF_4^-$ solution. Voltammograms start at the OCP towards the cathodic region (blue line) and anodic region (red line).

The CVs obtained with the aminoazobenzene **1a** are shown in Figure 7. The oxidation peak, at approximately 1.5 V (peak C), may be attributed to the oxidation of the ketone to a ketone radical cation, as explained in Figure 4. This peak's shape and potential are similar to those observed in Figure 4. When the oxidation peak C at 1.5 V is absent (CV, green line, Figure 7), the peak F1 at approximately −2.0 V (blue and red lines) is also not observed (green line), indicating that this peak F1 corresponds to the reduction of the ketone, as mentioned in Figure 4. Similarly, based on previous CVs, the oxidation peak D2 at approximately 1 V is attributed to the oxidation of the amine, as explained in Figure 5. The reduction peak F2 observed at −1.15 V may correspond to the reduction of the double bond in the azo group, from N=N to HN-NH.

Figure 8 shows the CVs of compound **2a**. Due to the proximity of the potential where the oxidation of the carbonyl can be observed in previous figures, the oxidation peak C at 1.7 V may be attributed to the same process. Meanwhile, the reduction peaks at −1 V (F2) and −2 V (F1) are due to the reduction of the azo group and the reduction of carbonyl, respectively, as mentioned previously. In this case, two oxidative processes are observed at 1.2 V (peak G1) and 1.36 V (peak G2). As can be seen, these peaks depend on the reduction of the azo moiety. As the potential range decreases from −2.2 V (blue line) to −1.5 (green line), −0.7 V (black line), and, finally, to −0.4 V (yellow line), the oxidation peaks disappear,

indicating that these peaks are due to the oxidation of HN-NH during the reduction of N=N. For this reason, there are two oxidation peaks, one for the oxidation of each "NH", with the following steps: HN-NH → •N-NH (oxidation peak G1) → •N-N• (oxidation peak G2) → N=N.

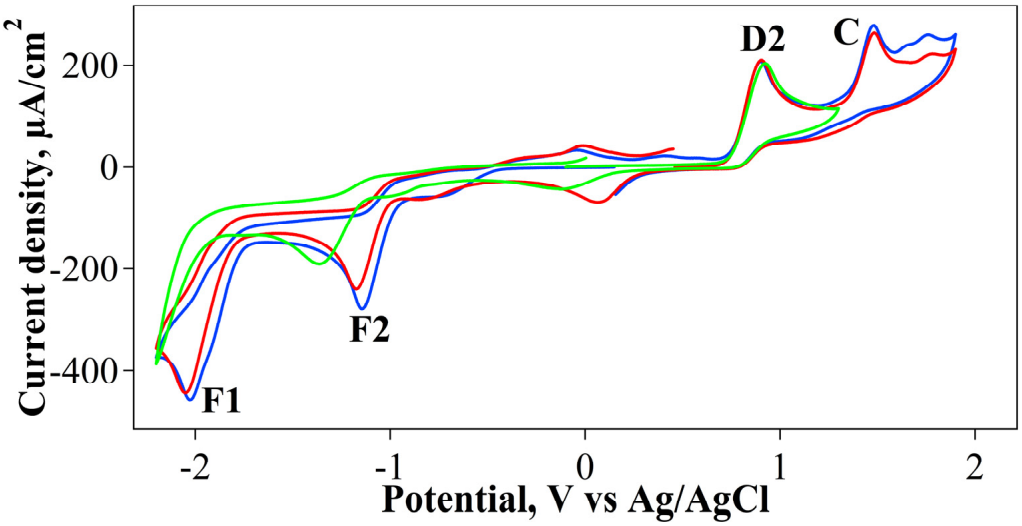

Figure 7. CV of aminoazobenzene **1a** in an MeCN + 0.1 M $TBABF_4^-$ solution. Voltammograms start at the OCP towards the cathodic region (blue line) and anodic region (red line) with a potential window from −2.2 V to 1.9 V. Green line: CV initiates towards the cathodic region with a potential window from 1.3 V to −2.2 V.

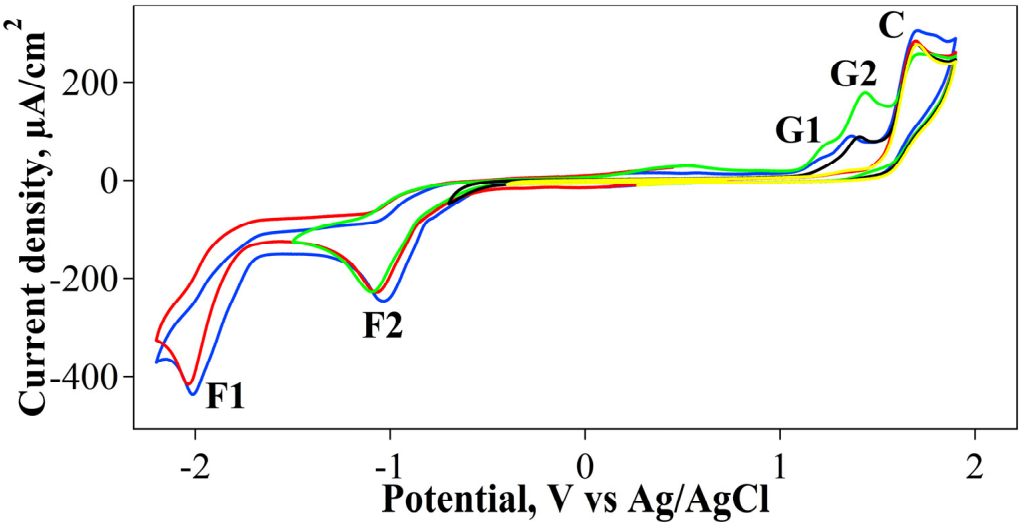

Figure 8. CV of compound **2a** in an MeCN + 0.1 M $TBABF_4^-$ solution. Voltammograms start at the OCP towards the cathodic region (blue line) and anodic region (red line) with a potential window from −2.2 V to 1.9 V. Subsequent CVs initiate towards the cathodic region with the following potential windows: −1.5 V to 1.9 V (green line) and −0.7 V to 1.9 V (yellow line).

Finally, in Figure 9, the remaining compounds of the series under study are shown. In each case, the same redox processes observed thus far are present, except for the reduction process observed at approximately −0.7 V (peak H) for compound **3d** (gray line), which is likely due to the reduction of the nitro group (NO_2) to the hydroxylamine group, as reported by Sadatnabi et al. [73].

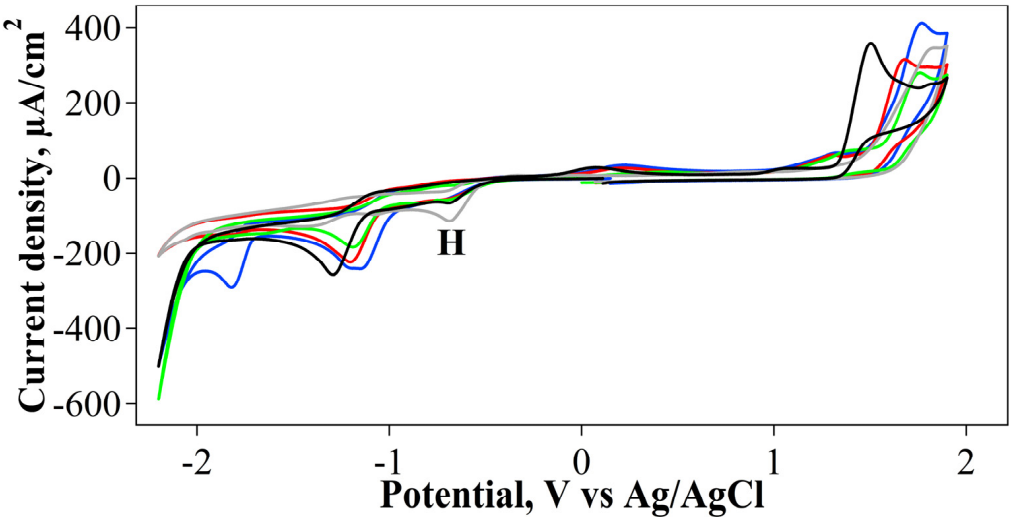

Figure 9. CVs obtained in an MeCN + 0.1 M $TBABF_4^-$ solution initiated at the OCP towards the cathodic region for compound **3b** (blue line), compound **3c** (red line), compound **3d** (gray line), compound **3e** (black line), and compound **3f** (green line).

4. Conclusions

The synthesis of six new azobenzene maleimide derivatives from 4-aminoazobenzenes and maleic anhydride was carried out in a two-step process. The aminoazobenzene derivatives were prepared via a classical diazotization-coupling reaction, using 3,5-dimethylaniline as the coupling agent. With the *N*-azobenzene maleimide compounds, a Dies–Alder cycloaddition reaction was performed to obtain six new *exo-N*-azobenzene oxa-norbornene dicarboximides. The IR and NMR spectroscopy results were consistent with the chemical structures resulting from the transformation of the compounds.

The electrochemical study of the organic compounds using cyclic voltammetry revealed valuable insights into their redox behavior. By analyzing the oxidation and reduction peaks, it was possible identify the specific electrochemical processes and determine the stability and reactivity of the compounds, as well as the reaction products. In this context, the analyses showed that these compounds underwent a series of electron transfer reactions primarily associated with the azo and carbonyl groups. This is because the reduction and hydrogenation of a double bond is a thermodynamically stable reaction, leading to the formation of lower-energy products. Similarly, it was observed that amines were the most electrochemically active functional groups in compounds that did not contain azo or carbonyl groups, such as some of the raw materials used. In these cases, amine oxidations predominantly occurred, forming radical cations which likely led to the formation of azo-containing compounds. Additionally, the reduction of carbonyl groups, where radical compounds are likely generated, could result in polymers as the reaction products. For all these reasons, electrochemical methods applied to organic compounds are of particular importance because they can facilitate and/or optimize the synthesis of novel products, such as the polymers mentioned in this study. For this reason, the electrochemical technique is proven to be a powerful tool for understanding the electron transfer mechanisms and potential applications of organic molecules in various fields, such as materials science and synthesis.

Finally, our electrochemical studies pave the way for future research aimed at expanding the scope of this investigation to further elucidate the reaction products formed under various electrochemical conditions. These additional studies will provide a deeper understanding of the reactivity and potential applications of these compounds.

Supplementary Materials: The following supporting information can be downloaded at https://www.mdpi.com/article/10.3390/reactions5040049/s1: Figure S1: Assignments of 1H NMR peaks of compounds **1a**. Figure S2: Assignments of 13C NMR peaks of compounds **1a**. Figure S3: Assignments of 1H NMR peaks of compounds **1b**. Figure S4: Assignments of 13C NMR peaks of compounds **1b**. Figure S5: Assignments of 1H NMR peaks of compounds **1c**. Figure S6: Assignments of 13C NMR peaks of compounds **1c**. Figure S7: Assignments of 13C NMR peaks of compounds **1c**. Figure S8: Assignments of 13C NMR peaks of compounds **1d**. Figure S9: Assignments of 1H NMR peaks of compounds **1e**. Figure S10: Assignments of 13C NMR peaks of compounds **1e**. Figure S11: Assignments of 1H NMR peaks of compounds **1f**. Figure S12: Assignments of 13C NMR peaks of compounds **1f**. Figure S13: Assignments of 1H NMR peaks of compounds **2a**. Figure S14: Assignments of 13C NMR peaks of compounds **2a**. Figure S15: Assignments of 1H NMR peaks of compounds **2b**. Figure S16: Assignments of 13C NMR peaks of compounds **2b**. Figure S17: Assignments of 1H NMR peaks of compounds **2c**. Figure S18: Assignments of 13C NMR peaks of compounds **2c**. Figure S19: Assignments of 1H NMR peaks of compounds **2d**. Figure S20: Assignments of 13C NMR peaks of compounds **2d**. Figure S21: Assignments of 1H NMR peaks of compounds **2e.** Figure S22: Assignments of 13C NMR peaks of compounds **2e**. Figure S23: Assignments of 1H NMR peaks of compounds **2f**. Figure S24: Assignments of 13C NMR peaks of compounds **2f**. Figure S25: Assignments of 1H NMR peaks of compounds **3a**. Figure S26: Assignments of 13C NMR peaks of compounds **3a**. Figure S27: Assignments of 1H NMR peaks of compounds **3b**. Figure S28: Assignments of 13C NMR peaks of compounds **3b**. Figure S29: Assignments of 1H NMR peaks of compounds **3c**. Figure S30: Assignments of 13C NMR peaks of compounds **3c**. Figure S31: Assignments of 1H NMR peaks of compounds **3d**. Figure S32: Assignments of 13C NMR peaks of compounds **3d**. Figure S33: Assignments of 1H NMR peaks of compounds **3e**. Figure S34: Assignments of 13C NMR peaks of compounds **3e**. Figure S35: Assignments of 1H NMR peaks of compounds **3f**. Figure S36: Assignments of 13C NMR peaks of compounds **3f**. Figure S37: FTIR spectrum of compounds **2a**. Figure S38: FTIR spectrum of compounds **2b**. Figure S39: FTIR spectrum of compounds **2c**. Figure S40: FTIR spectrum of compounds **2d**. Figure S41: FTIR spectrum of compounds **2e.** Figure S42: FTIR spectrum of compounds **2f**. Figure S43: FTIR spectrum of compounds **3a**. Figure S44: FTIR spectrum of compounds **3b**. Figure S45: FTIR spectrum of compounds **3c**. Figure S46: FTIR spectrum of compounds **3d**. Figure S47: FTIR spectrum of compounds **3e**. Figure S48: FTIR spectrum of compounds **3f**. Figure S49: CV obtained with oxa-norbornene-5,6-dicarboxylic anhydride in a MeCN + 0.1 M $TBABF4^{-}$ solution. Voltammograms started at the OCP towards six cycles.

Author Contributions: Conceptualization, A.P.-C.; Methodology, D.F.V.-V., D.A.F.-H., A.P.-C. and J.M.F.-A.; Formal analysis, D.F.V.-V., D.A.F.-H., H.G.-O. and J.S.G.-G.; Investigation, D.A.F.-H., A.P.-C., J.M.F.-A., H.G.-O. and J.S.G.-G.; Writing—original draft, D.F.V.-V. and J.M.F.-A.; Writing—review & editing, A.P.-C., H.G.-O. and J.S.G.-G. All authors have read and agreed to the published version of the manuscript.

Funding: This Research was funded by CONAHCYT for the scholarship granted to CVU 1086404, Facultad de Química, UNAM, for grant no. PAIP 5000-9112 and Universidad de la Cañada, for grant UNCA-PFI 01/23.

Data Availability Statement: The original contributions presented in the research are included in the article. Any further inquiries may be directed to the corresponding author.

Acknowledgments: The authors are grateful to Facultad de Ciencias Químicas, Universidad de Colima, Mexico, Facultad de Química, UNAM, CDMX and Instituto de farmacobiologia, Universidad de la Cañada, Oaxaca, Mexico for their scientific support of this Research.

Conflicts of Interest: The authors declare no conflicts of interest.

References

1. Diels, O.; Alder, K. Synthesen in Der Hydroaromatischen Reihe. *Liebigs Ann. Chem.* **1928**, *460*, 98–122. [CrossRef]
2. Li, W.; Zhou, L.; Zhang, J. Recent Progress in Dehydro(Genative) Diels–Alder Reaction. *Chem. Eur. J.* **2016**, *22*, 1558–1571. [CrossRef]
3. Briou, B.; Améduri, B.; Boutevin, B. Trends in the Diels–Alder Reaction in Polymer Chemistry. *Chem. Soc. Rev.* **2021**, *50*, 11055–11097. [CrossRef]
4. Funel, J.; Abele, S. Industrial Applications of the Diels–Alder Reaction. *Angew. Chem. Int. Ed.* **2013**, *52*, 3822–3863. [CrossRef]

5. Gregoritza, M.; Brandl, F.P. The Diels–Alder Reaction: A Powerful Tool for the Design of Drug Delivery Systems and Biomaterials. *Eur. J. Pharm. Biopharm.* **2015**, *97*, 438–453. [CrossRef]
6. LaMondia, J.A.; Douglas, S.M. Sensitivity of *Botrytis cinerea* from Connecticut Greenhouses to Benzimidazole and Dicarboximide Fungicides. *Plant Dis.* **1997**, *81*, 729–732. [CrossRef]
7. Vetcher, L.; Menzella, H.G.; Kudo, T.; Motoyama, T.; Katz, L. The Antifungal Polyketide Ambruticin Targets the HOG Pathway. *Antimicrob. Agents Chemother.* **2007**, *51*, 3734–3736. [CrossRef]
8. Sun, J.; Pang, C.; Cheng, X.; Yang, B.; Jin, B.; Jin, L.; Qi, Y.; Sun, Y.; Chen, X.; Liu, W.; et al. Investigation of the Antifungal Activity of the Dicarboximide Fungicide Iprodione against Bipolaris Maydis. *Pestic. Biochem. Physiol.* **2023**, *190*. [CrossRef]
9. Sang, H.; Popko, J.T.; Chang, T.; Jung, G. Molecular Mechanisms Involved in Qualitative and Quantitative Resistance to the Dicarboximide Fungicide Iprodione in Sclerotinia Homoeocarpa Field Isolates. *Phytopathology* **2017**, *107*, 198–207. [CrossRef]
10. Yamaguchi, I.; Fujimura, M. Recent Topics on Action Mechanisms of Fungicides. *J. Pestic. Sci.* **2005**, *30*, 67–74. [CrossRef]
11. Ma, Z.; Qiu, S.; Zhang, D.; Guo, X.; Lu, Y.; Fan, Y.; Chen, X. Design, Synthesis, and Antifungal Activity of Novel Dithiin Tetracarboximide Derivatives as Potential Succinate Dehydrogenase Inhibitors. *Pest. Manag. Sci.* **2023**, *79*, 1922–1930. [CrossRef]
12. Singh, R.N.; Kumar, P.; Kumar, N.; Singh, D.K. Efficacy of binary combination of deltamethrin+MGK-264 on levels of biochemical changes in the snail lymnaea acuminata. *Int. J. Pharm. Pharm. Sci* **2020**, 111–116. [CrossRef]
13. Chen, L.H.; Wilson, M.E.; Schlagenhauf, P. Prevention of Malaria in Long-Term Travelers. *JAMA* **2006**, *296*, 2234. [CrossRef]
14. Katz, T.M.; Miller, J.H.; Hebert, A.A. Insect Repellents: Historical Perspectives and New Developments. *J. Am. Acad. Dermatol.* **2008**, *58*, 865–871. [CrossRef]
15. Hurley, P.M. Mode of Carcinogenic Action of Pesticides Inducing Thyroid Follicular Cell Tumors in Rodents. *Environ. Health Perspect.* **1998**, *106*, 437–445. [CrossRef]
16. Matsumoto, M.; Furukawa, M.; Kobayashi, K.; Iso, T.; Igarashi, T.; Yamada, T.; Hirose, A. A 28-Day Repeated Oral-Dose Toxicity Study of Insecticide Synergist N-(2-Ethylhexyl)-1-Isopropyl-4-Methylbicyclo [2.2.2] Oct-5-Ene-2,3-Dicarboximide in Rats. *Fundam. Toxicol. Sci.* **2018**, *5*, 1–11. [CrossRef]
17. Colt, J.S.; Cyr, M.J.; Zahm, S.H.; Tobias, G.S.; Hartge, P. Inferring Past Pesticide Exposures: A Matrix of Individual Active Ingredients in Home and Garden Pesticides Used in Past Decades. *Environ. Health Perspect.* **2007**, *115*, 248–254. [CrossRef]
18. Jones, B.A.; Ahrens, M.J.; Yoon, M.H.; Facchetti, A.; Marks, T.J.; Wasielewski, M.R. High-Mobility Air-Stable n-Type Semiconductors with Processing Versatility: Dicyanoperylene-3,4:9,10-Bis(Dicarboximides). *Angew. Chem. Int. Ed.* **2004**, *43*, 6363–6366. [CrossRef]
19. Chen, Z.; Debije, M.G.; Debaerdemaeker, T.; Osswald, P.; Würthner, F. Tetrachloro-Substituted Perylene Bisimide Dyes as Promising n-Type Organic Semiconductors: Studies on Structural, Electrochemical and Charge Transport Properties. *ChemPhysChem* **2004**, *5*, 137–140. [CrossRef]
20. Paterson, A.F.; Savva, A.; Wustoni, S.; Tsetseris, L.; Paulsen, B.D.; Faber, H.; Emwas, A.H.; Chen, X.; Nikiforidis, G.; Hidalgo, T.C.; et al. Water Stable Molecular N-Doping Produces Organic Electrochemical Transistors with High Transconductance and Record Stability. *Nat. Commun.* **2020**, *11*, 3004. [CrossRef]
21. Dai, G.; Chang, J.; Jing, L.; Chi, C. Diacenopentalene Dicarboximides as New N-Type Organic Semiconductors for Field-Effect Transistors. *J. Mater. Chem. C Mater.* **2016**, *4*, 8758–8764. [CrossRef]
22. Hayes, R.T.; Wasielewski, M.R.; Gosztola, D. Ultrafast Photoswitched Charge Transmission through the Bridge Molecule in a Donor-Bridge-Acceptor System. *J. Am. Chem. Soc.* **2000**, *122*, 5563–5567. [CrossRef]
23. Lukas, A.S.; Bushard, P.J.; Wasielewski, M.R. Ultrafast Molecular Logic Gate Based on Optical Switching between Two Long-Lived Radical Ion Pair States. *J. Am. Chem. Soc.* **2001**, *123*, 2440–2441. [CrossRef] [PubMed]
24. Alonso-Navarro, M.J.; Harbuzaru, A.; Martínez-Fernández, M.; Pérez Camero, P.; López Navarrete, J.T.; Ramos, M.M.; Ponce Ortiz, R.; Segura, J.L. Synthesis and Electronic Properties of Nitrogen-Doped π-Extended Polycyclic Aromatic Dicarboximides with Multiple Redox Processes. *J. Mater. Chem. C Mater.* **2021**, *9*, 7936–7949. [CrossRef]
25. Tomizaki, K.-y.; Loewe, R.S.; Kirmaier, C.; Schwartz, J.K.; Retsek, J.L.; Bocian, D.F.; Holten, D.; Lindsey, J.S. Synthesis and Photophysical Properties of Light-Harvesting Arrays Comprised of a Porphyrin Bearing Multiple Perylene-Monoimide Accessory Pigments. *J. Org. Chem.* **2002**, *67*, 6519–6534. [CrossRef]
26. Boobalan, G.; Imran, P.M.; Nagarajan, S. Self-Assembly and Optical Properties of N, N -Bis(4-(1-Benzylpiperidine)) Perylene-3,4,9,10-Tetracarboxylic Diimide. *Supramol. Chem.* **2012**, *24*, 238–246. [CrossRef]
27. Loewe, R.S.; Tomizaki, K.Y.; Youngblood, W.J.; Bo, Z.; Lindsey, J.S. Synthesis of Perylene-Porphyrin Building Blocks and Rod-like Oligomers for Light-Harvesting Applications. *J. Mater. Chem.* **2002**, *12*, 3438–3451. [CrossRef]
28. Abinaya, K.; Karthikaikumar, S.; Sudha, K.; Sundharamurthi, S.; Elangovan, A.; Kalimuthu, P. Synergistic Effect of 9-(Pyrrolidin-1-Yl)Perylene-3,4-Dicarboximide Functionalization of Amino Graphene on Photocatalytic Hydrogen Generation. *Sol. Energy Mater. Sol. Cells* **2018**, *185*, 431–438. [CrossRef]
29. Gregg, B.A.; Cormier, R.A. Doping Molecular Semiconductors: N-Type Doping of a Liquid Crystal Perylene Diimide. *J. Am. Chem. Soc.* **2001**, *123*, 7959–7960. [CrossRef]
30. Zhang, Z.; Gao, Y.; Li, Z.; Qiao, L.; Xiong, Q.; Deng, L.; Zhang, Z.; Long, R.; Zhou, Q.; Du, Y.; et al. Marked Passivation Effect of Naphthalene-1,8-Dicarboximides in High-Performance Perovskite Solar Cells. *Adv. Mater.* **2021**, *33*, 2008405. [CrossRef]

31. Al Kurdi, K.; McCarthy, D.P.; McMeekin, D.P.; Furer, S.O.; Tremblay, M.H.; Barlow, S.; Bach, U.; Marder, S.R. A Naphthalene Diimide Side-Chain Polymer as an Electron-Extraction Layer for Stable Perovskite Solar Cells. *Mater. Chem. Front.* **2021**, *5*, 450–457. [CrossRef]
32. Angadi, M.A.; Gosztola, D.; Wasielewski, M.R. Organic Light Emitting Diodes Using Poly(Phenylenevinylene) Doped with Perylenediimide Electron Acceptors. *Mater. Sci. Eng. B* **1999**, *63*, 191–194. [CrossRef]
33. Basyouni, M.Z.; Radwan, M.F.; Abdu, M.E.; Spring, A.M. Synthesis, Characterization, and Optical Properties of Carbazole-Functionalized Poly(Norbornene-Dicarboximide) by ROMP. *Evergreen* **2024**, *11*, 207–213. [CrossRef]
34. Huang, Z.; Bin, Z.; Su, R.; Yang, F.; Lan, J.; You, J. Molecular Design of Non-Doped OLEDs Based on a Twisted Heptagonal Acceptor: A Delicate Balance between Rigidity and Rotatability. *Angew. Chem. Int. Ed.* **2020**, *59*, 9992–9996. [CrossRef]
35. Nakaya, K.; Funabiki, K.; Shibata, K.; Matsui, M. Chiral *N*-Substituted Perylene-3,4-Dicarboximides as Fluorescent Labeling Reagents. *Bull. Chem. Soc. Jpn.* **2001**, *74*, 549–554. [CrossRef]
36. Wu, Z.H.; Zhu, X.; Yang, Q.; Zagranyarski, Y.; Mishra, K.; Strickfaden, H.; Wong, R.P.; Basché, T.; Koynov, K.; Bonn, M.; et al. Near-Infrared Perylenecarboximide Fluorophores for Live-Cell Super-Resolution Imaging. *J. Am. Chem. Soc.* **2024**, *146*, 7135–7139. [CrossRef]
37. Huth, K.; Heek, T.; Achazi, K.; Kühne, C.; Urner, L.H.; Pagel, K.; Dernedde, J.; Haag, R. Noncharged and Charged Monodendronised Perylene Bisimides as Highly Fluorescent Labels and Their Bioconjugates. *Chem. Eur. J.* **2017**, *23*, 4849–4862. [CrossRef] [PubMed]
38. Wang, D.; He, Y.; Deng, W.; Wang, X. The Photoinduced Surface-Relief-Grating Formation Behavior of Side-Chain Azo Polymers with Narrow Mr Distribution. *Dye Pigment.* **2009**, *82*, 286–292. [CrossRef]
39. Spiridon, M.C.; Iliopoulos, K.; Jerca, F.A.; Jerca, V.V.; Vuluga, D.M.; Vasilescu, D.S.; Gindre, D.; Sahraoui, B. Novel Pendant Azobenzene/Polymer Systems for Second Harmonic Generation and Optical Data Storage. *Dye. Pigment.* **2015**, *114*, 24–32. [CrossRef]
40. Zarins, E.; Balodis, K.; Ruduss, A.; Kokars, V.; Ozols, A.; Augustovs, P.; Saharovs, D. Molecular Glasses of Azobenzene for Holographic Data Storage Applications. *Opt. Mater.* **2018**, *79*, 45–52. [CrossRef]
41. Sun, B.; Ngai, J.H.L.; Zhou, G.; Zhou, Y.; Li, Y. Voltage-Controlled Conversion from CDS to MDS in an Azobenzene-Based Organic Memristor for Information Storage and Logic Operations. *ACS Appl. Mater. Interfaces* **2022**, *14*, 41304–41315. [CrossRef] [PubMed]
42. Fukuda, T. Rewritable High-Density Optical Recording on Azobenzene Polymer Thin Film. *Opt. Rev.* **2005**, *12*, 126–129. [CrossRef]
43. Xie, S.; Natansohn, A.; Rochon, P. Reviews Recent Developments in Aromatic Azo Polymers Research. *Chem. Mater.* **1993**, *5*, 403. [CrossRef]
44. Natansohn, A.; Rochon, P. Photoinduced Motions in Azo-Containing Polymers. *Chem. Rev.* **2002**, *102*, 4139–4175. [CrossRef] [PubMed]
45. Manea-Saghin, A.M.; Ion, A.E.; Kajzar, F.; Nica, S. Second Order Nonlinear Optical Properties of Poled Films Containing Azobenzenes Tailored with Azulen-1-Yl-Pyridine. *Heliyon* **2023**, *9*, e17360. [CrossRef]
46. Cuétara-Guadarrama, F.; Vonlanthen, M.; Sorroza-Martínez, K.; González-Méndez, I.; Rivera, E. Photoisomerizable Azobenzene Dyes Incorporated into Polymers and Dendrimers. Influence of the Molecular Aggregation on the Nonlinear Optical Properties. *Dye Pigment.* **2021**, *194*, 109551. [CrossRef]
47. Tonnelé, C.; Champagne, B.; Muccioli, L.; Castet, F. Nonlinear Optical Contrast in Azobenzene-Based Self-Assembled Monolayers. *Chem. Mater.* **2019**, *31*, 6759–6769. [CrossRef]
48. Iftime, G.; Lagugné Labarthet, F.; Natansohn, A.; Rochon, P.; Murti, K. Main Chain-Containing Azo-Tetraphenyldiaminobiphenyl Photorefractive Polymers. *Chem. Mater.* **2002**, *14*, 168–174. [CrossRef]
49. Tsutsumi, N. Recent Advances in Photorefractive and Photoactive Polymers for Holographic Applications. *Polym. Int.* **2017**, *62*, 167–174. [CrossRef]
50. Airinei, A.; Fifere, N.; Homocianu, M.; Gaina, C.; Gaina, V.; Simionescu, B.C. Optical Properties of Some New Azo Photoisomerizable Bismaleimide Derivatives. *Int. J. Mol. Sci.* **2011**, *12*, 6176–6193. [CrossRef]
51. Kienzler, M.A.; Reiner, A.; Trautman, E.; Yoo, S.; Trauner, D.; Isacoff, E.Y. A Red-Shifted, Fast-Relaxing Azobenzene Photoswitch for Visible Light Control of an Ionotropic Glutamate Receptor. *J. Am. Chem. Soc.* **2013**, *135*, 17683–17686. [CrossRef] [PubMed]
52. Wu, D.; Dong, M.; Collins, C.V.; Babalhavaeji, A.; Woolley, G.A. A Red-Light Azobenzene Di-Maleimide Photoswitch: Pros and Cons. *Adv. Opt. Mater.* **2016**, *4*, 1402–1409. [CrossRef]
53. Hien, L.T.; Schierling, B.; Ryazanova, A.Y.; Zatsepin, T.S.; Volkov, E.M.; Kubareva, E.A.; Velichko, T.I.; Pingoud, A.; Oretskaya, T.S. New Azobenzene Derivatives for Directed Modification of Proteins. *Russ. J. Bioorg Chem.* **2009**, *35*, 549–555. [CrossRef]
54. Venton, B.J.; Cao, Q. Fundamentals of Fast-Scan Cyclic Voltammetry for Dopamine Detection. *Analyst* **2020**, *145*, 1158–1168. [CrossRef] [PubMed]
55. Puthongkham, P.; Venton, B.J. Recent Advances in Fast-Scan Cyclic Voltammetry. *Analyst* **2020**, *145*, 1087–1102. [CrossRef]
56. Roberts, J.G.; Sombers, L.A. Fast-Scan Cyclic Voltammetry: Chemical Sensing in the Brain and Beyond. *Anal. Chem.* **2018**, *90*, 490–504. [CrossRef] [PubMed]
57. Alatraktchi, F.; Breum Andersen, S.; Krogh Johansen, H.; Molin, S.; Svendsen, W. Fast Selective Detection of Pyocyanin Using Cyclic Voltammetry. *Sensors* **2016**, *16*, 408. [CrossRef]
58. Espinoza, E.M.; Clark, J.A.; Soliman, J.; Derr, J.B.; Morales, M.; Vullev, V.I. Practical Aspects of Cyclic Voltammetry: How to Estimate Reduction Potentials When Irreversibility Prevails. *J. Electrochem. Soc.* **2019**, *166*, H3175–H3187. [CrossRef]

59. Petkovska, S.; Gulaboski, R. Theoretical Analysis of a Surface Catalytic Mechanism Associated with Reversible Chemical Reaction Under Conditions of Cyclic Staircase Voltammetry. *Electroanalysis* **2020**, *32*, 992–1004. [CrossRef]
60. Schindler, S.; Bechtold, T. Mechanistic Insights into the Electrochemical Oxidation of Dopamine by Cyclic Voltammetry. *J. Electroanal. Chem.* **2019**, *836*, 94–101. [CrossRef]
61. Sandford, C.; Edwards, M.A.; Klunder, K.J.; Hickey, D.P.; Li, M.; Barman, K.; Sigman, M.S.; White, H.S.; Minteer, S.D. A Synthetic Chemist's Guide to Electroanalytical Tools for Studying Reaction Mechanisms. *Chem. Sci.* **2019**, *10*, 6404–6422. [CrossRef] [PubMed]
62. Deshaies, S.; Garcia, L.; Veran, F.; Mouls, L.; Saucier, C.; Garcia, F. Red Wine Oxidation Characterization by Accelerated Ageing Tests and Cyclic Voltammetry. *Antioxidants* **2021**, *10*, 1943. [CrossRef] [PubMed]
63. José Jara-Palacios, M.; Luisa Escudero-Gilete, M.; Miguel Hernández-Hierro, J.; Heredia, F.J.; Hernanz, D. Cyclic Voltammetry to Evaluate the Antioxidant Potential in Winemaking By-Products. *Talanta* **2017**, *165*, 211–215. [CrossRef] [PubMed]
64. Wang, H.W.; Bringans, C.; Hickey, A.J.R.; Windsor, J.A.; Kilmartin, P.A.; Phillips, A.R.J. Cyclic Voltammetry in Biological Samples: A Systematic Review of Methods and Techniques Applicable to Clinical Settings. *Signals* **2021**, *2*, 138–158. [CrossRef]
65. Mitrasov, Y.N.; Avryuskaya, A.A.; Kondrat'eva, O.V. Condensation of Nitro- and Amino-Substituted Phenylmaleimides with Furfuryl Alcohol. *Russ. J. Gen. Chem.* **2015**, *85*, 75–78. [CrossRef]
66. Daeffler, C.S.; Miyake, G.M.; Li, J.; Grubbs, R.H. Partial Kinetic Resolution of Oxanorbornenes by Ring-Opening Metathesis Polymerization with a Chiral Ruthenium Initiator. *ACS Macro Lett.* **2014**, *3*, 102–104. [CrossRef]
67. France, M.B.; Alty, L.T.; Earl, T.M. Synthesis of a 7-Oxanorbornene Monomer: A Two-Step Sequence Preparation for the Organic Laboratory. *J. Chem. Educ.* **1999**, *76*, 659. [CrossRef]
68. Kamezawa, N.; Sakashita, K.; Hayamizu, K. Nuclear Magnetic Resonance Studies of 5,6-dicarboxy-2-norbornene Derivatives. *Org. Magn. Reson.* **1969**, *1*, 405–414. [CrossRef]
69. Vasudevan, D.; Wendt, H. Electroreduction of Oxygen in Aprotic Media. *J. Electroanal. Chem.* **1995**, *392*, 69–74. [CrossRef]
70. Sun, K.; Xu, Y.; Dumur, F.; Morlet-Savary, F.; Chen, H.; Dietlin, C.; Graff, B.; Lalevée, J.; Xiao, P. In Silico Rational Design by Molecular Modeling of New Ketones as Photoinitiators in Three-Component Photoinitiating Systems: Application in 3D Printing. *Polym. Chem.* **2020**, *11*, 2230–2242. [CrossRef]
71. Sharma, L.R.; Manchanda, A.K.; Singh, G.; Verma, R.S. Cyclic Voltammetry of Aromatic Amines in Aqueous and Non-Aqueous Media. *Electrochim. Acta* **1982**, *27*, 223–233. [CrossRef]
72. Akbulut, U.; Hacioğlu, B. Electronitiated Polymerization of Maleic Anhydride by Direct Electron Transfer. *J. Polym. Sci. A Polym. Chem.* **1991**, *29*, 219–224. [CrossRef]
73. Sadatnabi, A.; Mohamadighader, N.; Nematollahi, D. Convergent Paired Electrochemical Synthesis of Azoxy and Azo Compounds: An Insight into the Reaction Mechanism. *Org. Lett.* **2021**, *23*, 6488–6493. [CrossRef] [PubMed]